AD-A014 427

MAPPING OF SEA SURFACE TEMPERATURE BY THE DMSP SATELLITE

James L. Cogan, et al

Environmental Research and Technology, Incorporated

Prepared for:

Environmental Prediction Research Facility (Navy)

May 1975

DISTRIBUTED BY:

NTIS

National Technical Information Service
U. S. DEPARTMENT OF COMMERCE

Approved for Public Release:
Distribution Unlimited

EPRF 7-75 (ERT)

259085

ADA014427

MAPPING OF SEA SURFACE TEMPERATURE BY THE DMSP SATELLITE

ERT Document No. 1065

Final Report

May 1975

JAMES L. COGAN

JAMES H. WILLAND

DDC
RECEIVED
SEP 3 1975
D

prepared for

ENVIRONMENTAL PREDICTION RESEARCH FACILITY
NAVAL POST GRADUATE SCHOOL
MONTEREY, CALIFORNIA 93940

ENVIRONMENTAL RESEARCH & TECHNOLOGY, INC.
696 VIRGINIA ROAD, CONCORD, MASSACHUSETTS 01742 (617) 369-8910

Unclassified

SECURITY CLASSIFICATION OF THIS PAGE *(When Data Entered)*

REPORT DOCUMENTATION PAGE		READ INSTRUCTIONS BEFORE COMPLETING FORM
1. REPORT NUMBER EPRF 7-75 (ERT)	2. GOVT ACCESSION NO.	3. RECIPIENT'S CATALOG NUMBER
4. TITLE *(and Subtitle)* Mapping of Sea Surface Temperature by the DMSP Satellite		5. TYPE OF REPORT & PERIOD COVERED Final 6. PERFORMING ORG. REPORT NUMBER 1065
7. AUTHOR(s) James L. Cogan James H. Willand		8. CONTRACT OR GRANT NUMBER(s) 66856-4120-5502
9. PERFORMING ORGANIZATION NAME AND ADDRESS Environmental Research & Technology, Inc. 696 Virginia Road Concord, MA 01742		10. PROGRAM ELEMENT, PROJECT, TASK AREA & WORK UNIT NUMBERS W37-13; EPRF Wu 054:3-5
11. CONTROLLING OFFICE NAME AND ADDRESS Environmental Prediction Research Facility Naval Post Graduate School Monterey, CA 93940		12. REPORT DATE May 1975 13. NUMBER OF PAGES 82
14. MONITORING AGENCY NAME & ADDRESS*(if different from Controlling Office)*		15. SECURITY CLASS. *(of this report)* Unclassified 15a. DECLASSIFICATION/DOWNGRADING SCHEDULE
16. DISTRIBUTION STATEMENT *(of this Report)* Unlimited Distribution		
17. DISTRIBUTION STATEMENT *(of the abstract entered in Block 20, if different from Report)*		
18. SUPPLEMENTARY NOTES		
19. KEY WORDS *(Continue on reverse side if necessary and identify by block number)* Remote Sensing Sea Surface Temperature Infrared Radiation Mapping Algorithm Radiative Transfer Temperature Deficit Atmospheric Attenuation Satellite Measurements		

20. ABSTRACT *(Continue on reverse side if necessary and identify by block number)*

Sea surface temperature (T_S) may be inferred from Defense Meteorological Satellite Program (DMSP) satellite measurements of infrared radiances in atmospheric windows if errors in instrumentation, data processing, and satellite orientation are properly accounted for. The difference between T_S and the temperature inferred from satellite measurements of "window" radiances when looking vertically through a cloud-free atmosphere, herein called the deficit, may be computed by a simple parametric formula to $< \pm 1°K\ atm^{-1}$ of the value calculated

DD FORM 1 JAN 73 1473 EDITION OF 1 NOV 65 IS OBSOLETE

Unclassified

SECURITY CLASSIFICATION OF THIS PAGE *(When Data Entered)*

20. Abstract (cont)

by a numerical integration of the equation of radiative transfer. Unfortunately, serious discrepancies in the data from the DMSP (OLS-5D2) radiometer prevented a conclusive comparison between satellite and ship values of T_s.

Nevertheless, a mapping program was developed in anticipation of future data more suited for the inference of T_s. It was shown that an effective resolution, the area represented by each mapped value of T_s, of about 13 x 13 km may be attained close to the sub-satellite track under nearly cloud-free conditions. Furthermore, output from the mapping program suggested that T_s may be mapped to about ± 2°K with present DMSP data provided that some apparent discrepancies are accounted for.

Approved for Public Release:
Distribution Unlimited

EPRF 7-75 (ERT)

MAPPING OF SEA SURFACE TEMPERATURE BY THE DMSP SATELLITE

ERT Document No. 1065

Final Report

May 1975

JAMES L. COGAN
JAMES H. WILLAND

D D C
RECEIVED
SEP 3 1975
D

prepared for
ENVIRONMENTAL PREDICTION RESEARCH FACILITY
NAVAL POST GRADUATE SCHOOL
MONTEREY, CALIFORNIA 93940

ENVIRONMENTAL RESEARCH & TECHNOLOGY, INC
696 VIRGINIA ROAD CONCORD MASSACHUSETTS 01742 (617) 369 8910

ABSTRACT

Sea surface temperature (T_s) may be inferred from Defense Meteorological Satellite Program (DMSP) satellite measurements of infrared radiances in atmospheric windows if errors in instrumentation, data processing, and satellite orientation are properly accounted for. Even in the absence of clouds, the slight opacity of the atmosphere in the "windows" causes the temperature "seen" by the satellite to be lower than that measured by ships or aircraft. Clouds produce the same effect, but generally of a greater magnitude.

The difference between T_s and the temperature inferred from satellite measurements of "window" radiances when looking vertically through a cloud-free atmosphere, herein called the deficit, may be computed by a simple parametric formula to $< \pm 1°K\ atm^{-1}$ of the value calculated by a numerical integration of the equation of radiative transfer. Unfortunately, serious discrepancies in the data from the DMSP (OLS-5D2) radiometer prevented a conclusive comparison between satellite and ship values of T_s.

Nevertheless, a mapping program was developed in anticipation of future data more suited for the inference T_s. It was shown that an effective resolution, the area represented by each mapped value of T_s, of about 13 x 13 km may be attained close to the sub-satellite track under nearly cloud-free conditions. Furthermore, output from the mapping program suggested that T_s may be mapped to about $\pm 2°K$ with present DMSP data provided that some apparent discrepancies are accounted for.

ACKNOWLEDGMENTS

The authors wish to acknowledge the assistance provided for this project by Mr. Roland Nagle and others at EPRF. We also wish to thank the many helpful people at NOAA, ONR, WHOI and Westinghouse Electric Corp. for their timely assistance during a number of private communications. Other organizations that supplied data include the National Climatic Center of the Environmental Data Service (NOAA) and the Massachusetts Institute of Technology.

TABLE OF CONTENTS

		Page
ABSTRACT		iii
ACKNOWLEDGMENTS		iv
1.	INTRODUCTION	1
2.	DATA PROCESSING	3
3.	SOURCES OF ERROR	15
	3.1 Earth Location	15
	3.2 Calibration Procedures	16
	3.3 'Skin' Effect and Accuracy of Ship Measurements	18
	3.4 Emissivity of the Sea Surface	19
	3.5 Signal Noise and Random Error	19
4.	THE CLOUD PROBLEM	23
	4.1 Relationship Between Visible Brightness and Radiance Temperature	24
	4.2 Delineation of Cloud	26
5.	THE DEFICIT, A CORRECTION FOR ATMOSPHERIC ATTENUATION	28
	5.1 Primary Absorbers and Model Atmospheres	28
	5.2 Computation of the Deficit	31
	5.3 A Parametric Formula	35
	5.4 Measurement of Integrated Water Vapor by NEMS and Radiosonde	41
	5.5 Approximate Estimates	43
	5.5.1 The Deifcit as a Function of Measured Radiance Temperature	43
	5.5.2 Statistical Estimate	45
	5.6 Comparison of Computed with Observed Deficits	47
6.	MAPPING RESULTS	55
	6.1 Comparison of Daily Maps	55
	6.2 Effect of a Variable Zenith Angle	62
	6.3 Variation of Effective Resolution	64
	6.4 Quality and Limitations	69
7.	CONCLUSION	71

1. INTRODUCTION

Sea surface temperature may be inferred from satellite measurements of infrared radiances in the atmospheric windows. The slight opacity of the atmosphere in infrared "windows" caused by absorption by water vapor, ozone, carbon dioxide and extinction by aerosols causes the temperature observed by the satellite to be lower than that of the sea surface, even when errors arising from instrumentation, data processing, and satellite orientation have been accounted for. Clouds in the instantaneous field-of-view (IFOV) of the radiometer produce the same effect, but generally of a larger magnitude.

Other investigations have inferred sea surface temperature (T_s) to varying degrees of accuracy using data from satellites. Smith et al (1970) developed a statistical technique for obtaining T_s which gave accuracies of about ± 1°K for a 1° latitude grid using 3.8 μm data from the High Resolution Infrared Radiometer (HRIR) of Nimbus 2. Maul and Sidran (1973) estimated errors of about 2°K in T_s for scanning radiometer data from the NOAA satellites. Stevenson et al (1972) presented maps of T_s measured by ship and satellite (NOAA-1) that may be compared to estimate the accuracy of the satellite values relative to the ship measurements. For cloud-free areas of about 80 x 80 km, a mean accuracy in T_s of about ± 1 to 1.5°K was attained for the "Little Window 2" region near the southern end of the Gulf of California in May 1971. Cogan and Willand (1974) developed an automated technique that enabled T_s to be mapped to an accuracy of about ± 1°K for cloud-free areas of about 40 x 40 km using NOAA-2 data. Prabhakara et al (1974) suggested utilizing a dual-channel radiometer operating in the 11-13 μm "window" to infer T_s, where the differential absorption is used to derive a correction for atmospheric attenuation. In a test of their method using IRIS data from the Nimbus 3 and 4 satellites, they found an agreement of about ± 1°K with ship measurements.

In this study observation of T_s was restricted, as far as could be established, to IFOV's that were free of clouds. Scan spots for areas with overcast, broken, or thickly scattered (many small elements close together) cloud cover were eliminated by a technique utilizing both

visible and infrared data. The problem of a few scattered low clouds was overcome by averaging a sufficiently large number of radiance temperatures that lay within limits prescribed by climatology.

Radiances were measured by the scanning radiometer carried on Block 5C Defense Meteorological Satellite Program (DMSP) satellites. This instrument has four channels with the following specifications:

	Channel	Spectral Interval	IFOV*
High Resolution (HR)	Visible	0.4 - 1.1 μm	2.0 nmi (3.7 km)
	Infrared	7.7 - 13.1 μm	2.3 nmi (4.3 km)
Very High Resolution (VHR)	Visible	0.4 - 1.1 μm	0.33 nmi (0.61 km)
	Infrared	7.9 - 13.1 μm	0.35 nmi (0.65 km)

*IFOV based on an orbital altitude of 434 nmi (804 km).

The infrared data used in this study were taken from the HR sensor and the visible data from the VHR sensor. The response curve of the HR infrared sensor has a peak near the center of the 9.6 μm ozone absorption band (Spangler, 1974), thereby increasing the difficulty of interpreting the data. Furthermore, this sensor is sensitive to radiation affected by absorption by N_2O and CH_4 near 8 μm and by wings of the 6.7 μm water vapor and 15 μm carbon dioxide bands.

In the present study, a correction for atmospheric attenuation is devised that is computed in terms of atmospheric parameters. The theory behind the correction for continuum absorption by water vapor was originally developed by Bignell (1970) and further developed and verified by Cogan (1972), Platt (1972), and Cogan and Willand (1974). Computations of attenuation by other gases and aerosols were based on work by McClatchey et al (1972) and Selby and McClatchey (1972).

An automated mapping algorithm is developed in which each mapped T_s represents an area of only about 13 x 13 km near the sub-satellite track under favorable atmospheric conditions. It appears that T_s may be inferred to an accuracy of about ± 2°K provided that some apparent discrepancies in the data are accounted for.

The results of this study, and the algorithms developed, are presented in subsequent sections of this report.

2. DATA PROCESSING

The processed and analyzed data were measured by the DMSP satellite over the Mid-Ocean Dynamics Experiment (MODE) area centered near 28°N, 69° 40'W. This region was selected because of the availability of ground truth measurements from ships and aircraft participating in the MODE. Data over this region was made available to the study by the Environmental Prediction Research Facility (EPRF) These included.

- A tape of digitized infrared and visible data from the high resolution and very high resolution radiometer respectively from the DMSP satellite;
- Infrared and visible imagery of the data and DMSP satellite photographs for the same dates;
- Ground truth measurements of T_s and radiosonde ascents from ships (CHAIN, EASTWIND, HUNT, and RESEARCHER) participating in the MODE.
- One set of dropsonde data.

The period of record by date of each tape is indicated by the following list:

Tape Number	Date
1	13 June 1973
2	14 June 1973
3	15 June 1973

Three types of data records appear on each tape for each group of scan lines, where six scan lines of visible data were followed by a corresponding single scan line of infrared temperature and calibration data. At the beginning of each record was an identification portion indicating date, time, location, etc. of the scan line. The data portion of each visible scan line consisted of 3400 scan spots, each spot a 6-bit binary integer where 0 corresponds to black and 63 to white. Scan lines of infrared data contained 700 scan spots, each spot a 24-bit binary integer giving temperature in °C x 10.

Three separate programs were developed for processing of the taped data. Figure 2.1 summarizes the three programs developed for the data selection, extraction, and utilization.

The first program extracted infrared and visible scan lines over selected areas and printed the data in a format suitable for rapid examination. Card input to the program contained starting and ending scan line numbers that were determined from imagery of the data over the areas of concern. Due to the difference in IFOV between the visible and infrared sensors, a scheme was developed and incorporated into the program to compress the very high resolution visible data down to about the resolution of the infrared data.

From tape dumps of the infrared data, it was determined that out of 700 scan spots within a single scan line, only 620 scan spots were actually viewing the earth; of 3400 visible scan spots, only 3330 were viewing the earth. Therefore, the program had to compress 3330 visible scan spots to match 620 infrared scan spots. After a scan line of visible data was read in, the first four groups of five visible data responses each were entered into the first four words of a 620-element array. The program then proceeded to enter a sequence of five, six, and five visible data responses into the array, switching the sequence to five, six, and six data elements every 24th time until 617 array elements were filled. The final three elements in the 620-element array were filled with a sequence of five, five, and five visible values. This procedure was continued until six visible scan lines were processed. For each element of the array, the sum of visible brightness values was then divided by the population of visible data, thereby producing the final compressed brightness (i.e., averaged value of 30 or 36 visible scan spots). Figure 2.2 illustrates the procedure. The final values were then changed to alphanumeric characters and printed to form a pattern map of visible scan lines. The alphanumeric characracters for the averaged visible data are shown in Table 2.1. A pattern map of infrared scan lines over the same area was also produced where radiance temperatures less than 8.5°C were represented by an asterisk and all others by a '0'. Analyzed cloud cover patterns in each output were then used to position ship locations. Figure 2.3 illustrates a very small segment of the printout of the visible and

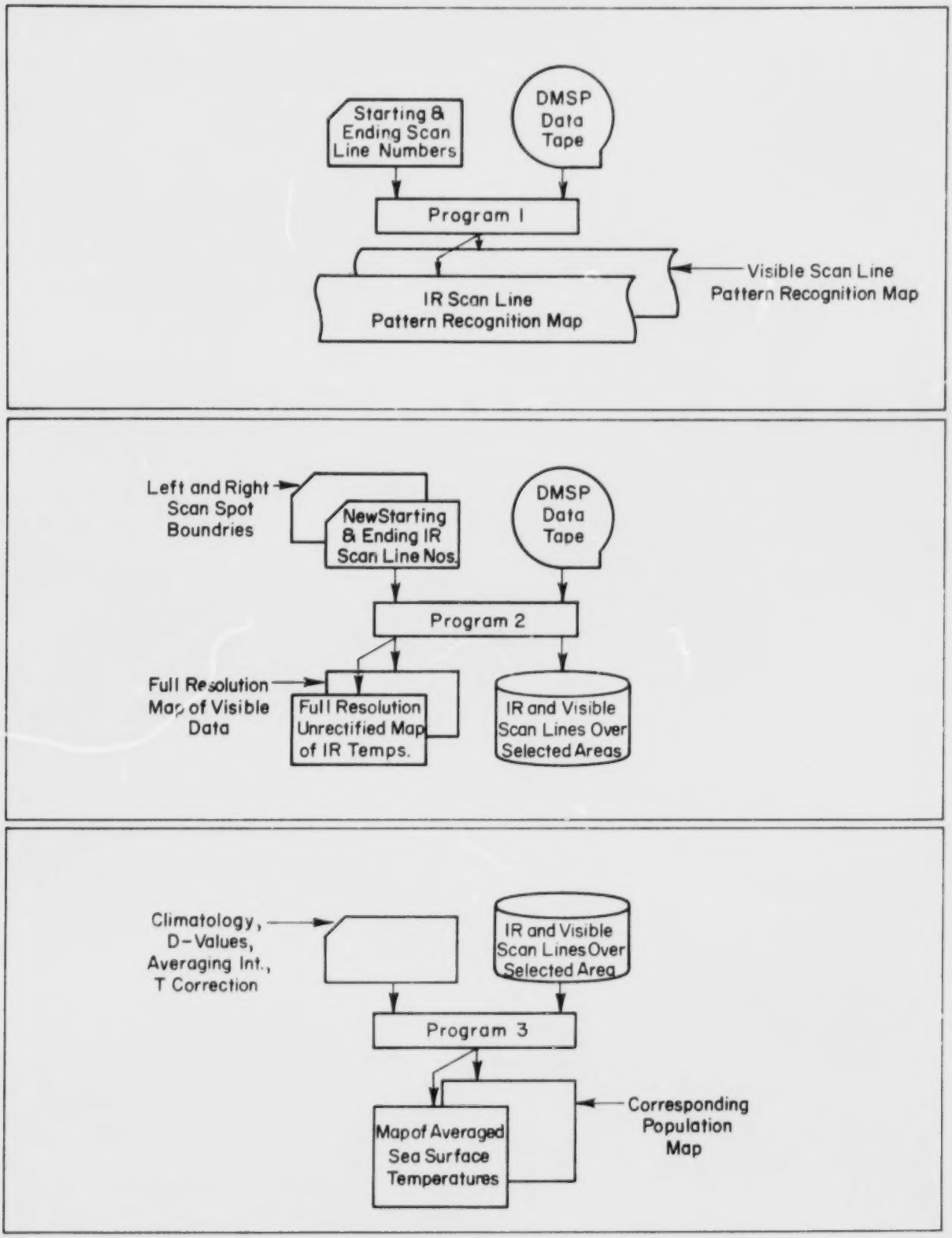
Starting & Ending Scan Line Numbers
DMSP Data Tape
Program 1
IR Scan Line Pattern Recognition Map
Visible Scan Line Pattern Recognition Map
Left and Right Scan Spot Boundries
NewStarting & Ending IR Scan Line Nos.
DMSP Data Tape
Program 2
Full Resolution Map of Visible Data
Full Resolution Unrectified Map of IR Temps.
IR and Visible Scan Lines Over Selected Areas
Climatology, D-Values, Averaging Int., T Correction
IR and Visible Scan Lines Over Selected Areg
Program 3
Map of Averaged Sea Surface Temperatures
Corresponding Population Map

Figure 2.1 Schematic diagrams of the data processing programs.

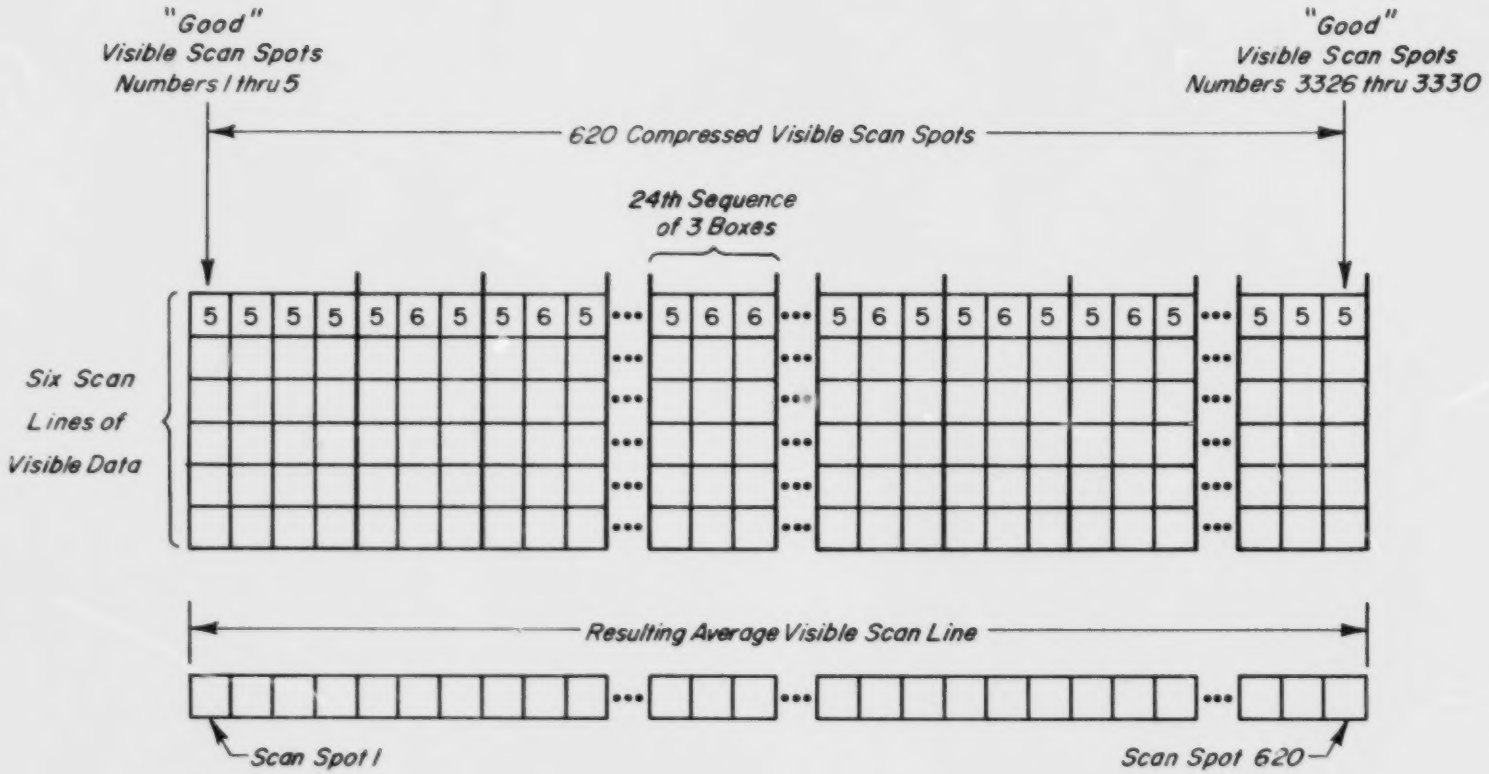
"Good"
Visible Scan Spots
Numbers 1 thru 5
"Good"
Visible Scan Spots
Numbers 3326 thru 3330
620 Compressed Visible Scan Spots
24th Sequence
of 3 Boxes
Six Scan
Lines of
Visible Data
5 5 5 5 5 6 5 5 6 5 ... 5 6 6 ... 5 6 5 5 6 5 5 6 5 ... 5 5 5
Resulting Average Visible Scan Line
Scan Spot 1
Scan Spot 620

Figure 2.2 Schematic diagram of the method used to compress visible data to a resolution similar to that of infrared data.

TABLE 2.1

SCHEME FOR CONVERSION OF VISIBLE BRIGHTNESS (b)
TO ALPHANUMERIC CODE. UNITS OF b ARE DIGITAL COUNTS

Blank	$0<b<8$
1	$8\leq b<16$
2	$16\leq b<24$
3	$24\leq b<32$
4	$32\leq b<40$
5	$40\leq b<48$
6	$48\leq b<56$
7	$56\leq b<64$

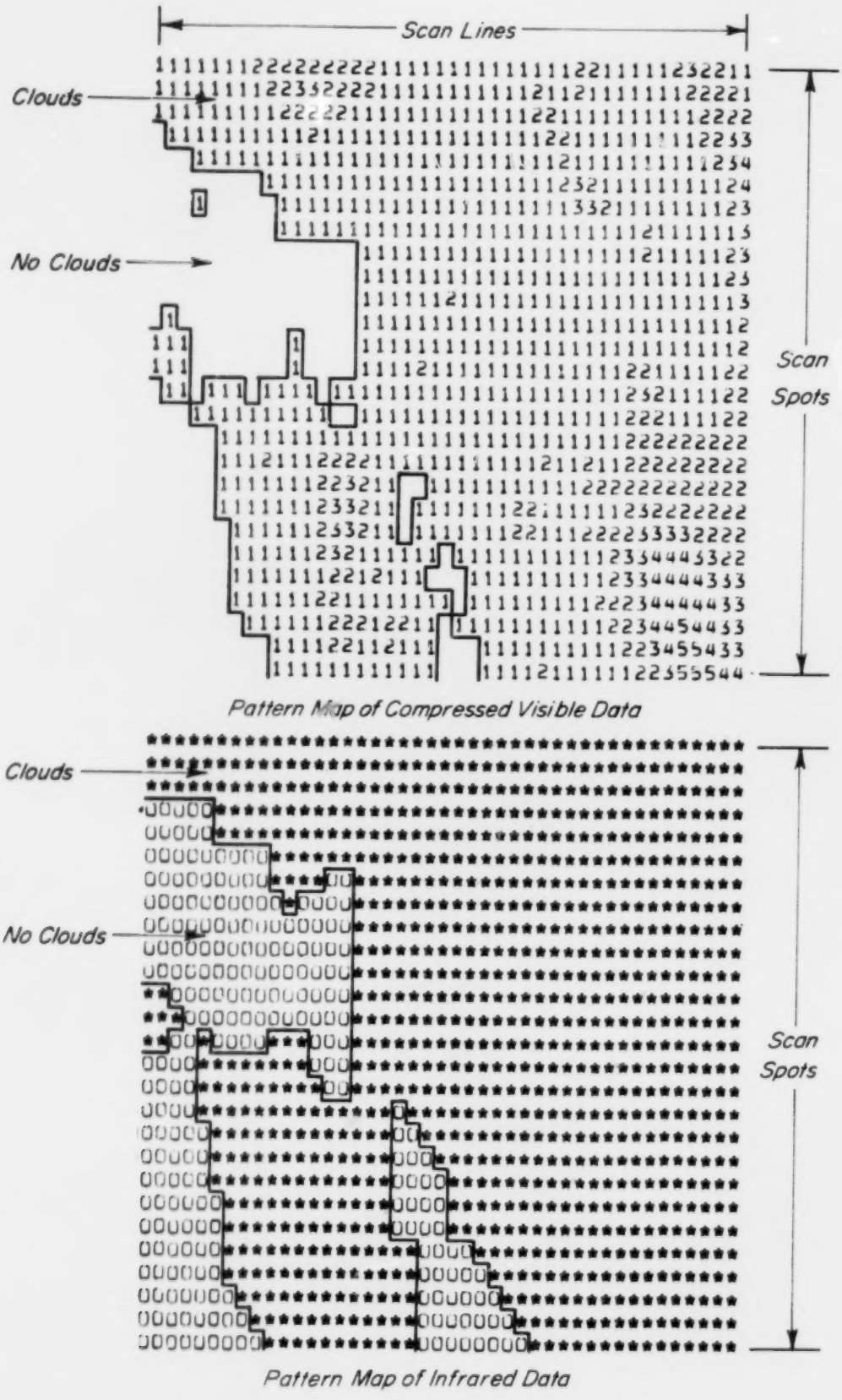

Figure 2.3 Sample sections of the pattern recognition maps produced by 1.

corresponding infrared scan lines for 14 June 1973. After outlining cloud patterns and plotting ship positions, the left and right most scan spots were determined, thereby defining the area encompassing the ships. The chosen scan spot numbers together with selected scan lines were used in the following two programs.

The second program was designed to read in data over the area selected in the first step and output them in the form of full resolution maps of infrared temperatures and compressed visible data values for detailed hand analysis. The infrared and visible scan lines selected by the program were stored on a sequential disk data set for further processing using program number three. Sections of hand analyzed maps of infrared temperatures and visible data for 14 June 1973 over Ship R are shown in Figures 2.4 and 2.5.

Each infrared temperature printed in Figure 2.4 represents a value of equivalent black body temperature (T_B) x 10 with the first digit not printed (e.g., 886 = 288.6°K). Data printed as zero are for missing scan spots.

The third program was designed to read in the data stored on disk by the second program, operate on them, and produce maps of various sizes. Inserted into the program were some predetermined equations derived from the geometry of the DMSP satellite for computing the zenith angle associated with each scan spot along a scan line (see Figure 2.6a). The maximum nadir angle (η_m) was pre-computed to be 62.6 degrees by:

$$\eta_m = \sin^{-1} \frac{R}{R+h}$$

where R = radius of the earth (6371 km) and h = altitude of the satellite (804.5 km). The zenith angle (z) of any scan spot along a scan line can be computed by:

$$z = (\sin^{-1} \frac{R+h}{R} \sin \eta)$$

where η = nadir angle.

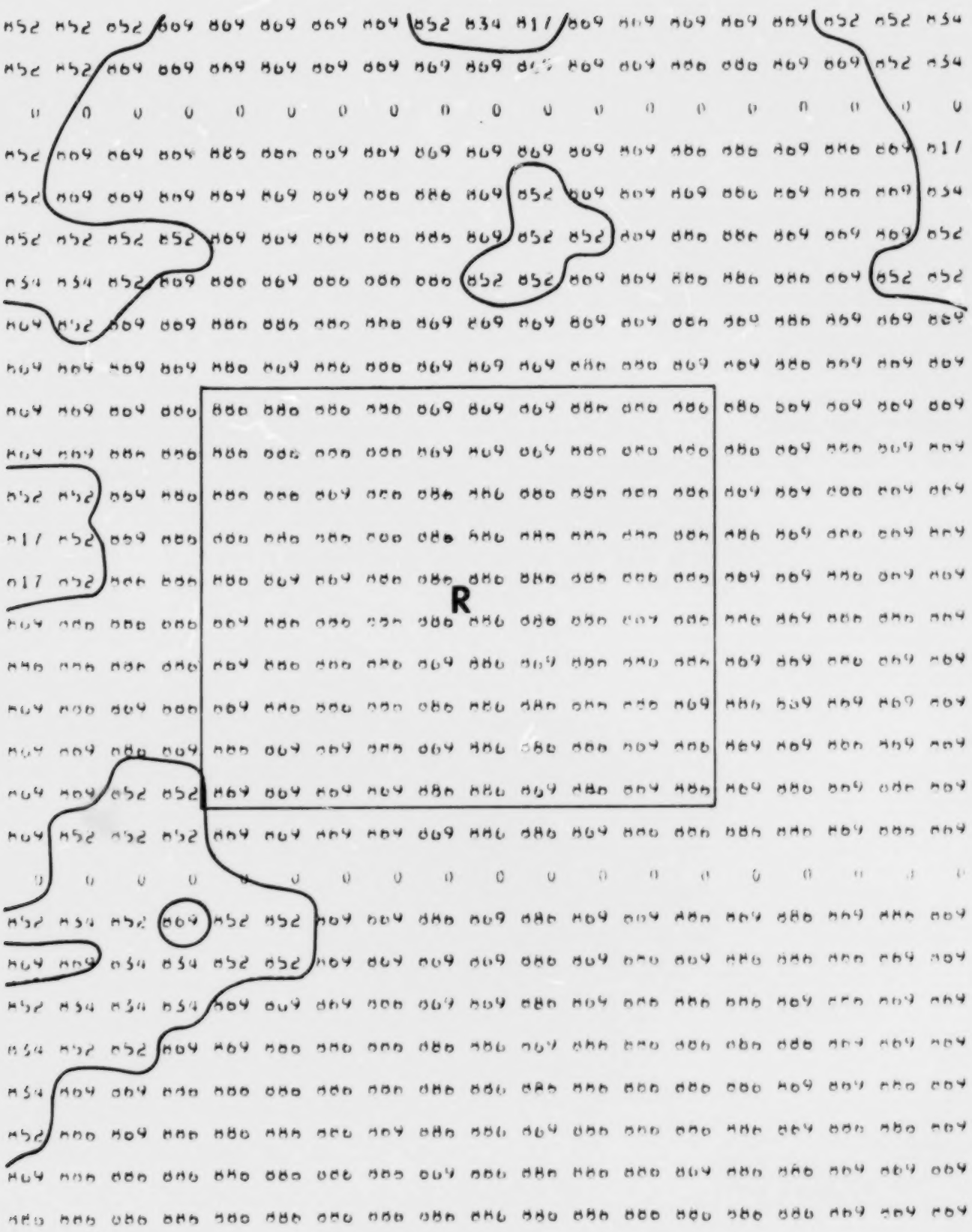

Figure 2.4 A section of the map of T_B for 14 June 1973. Plotted values are in °K x 10 with the first digit not printed (i.e., 886 = 288.6°K). Compare with Figure 2.5.

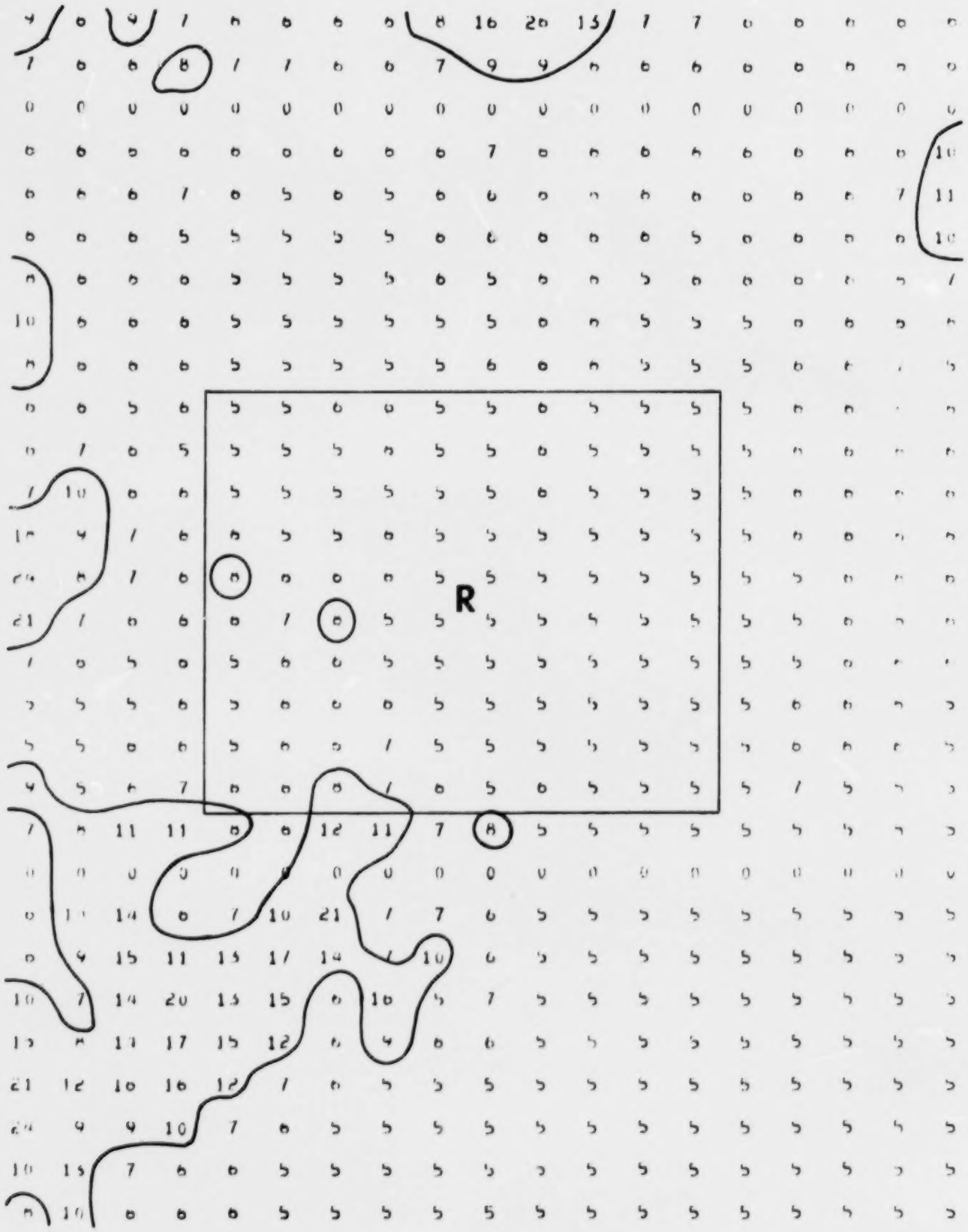

751122

Figure 2.5 A section of the map of b for 14 June 1973. Plotted values are in digital counts. Compare with Figure 2.4.

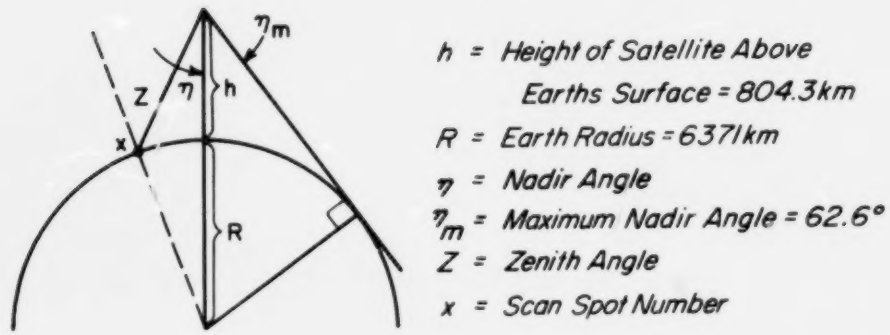

Figure 2.6a Geometry used for computing the zenith angle for a given scan spot along a scan line.

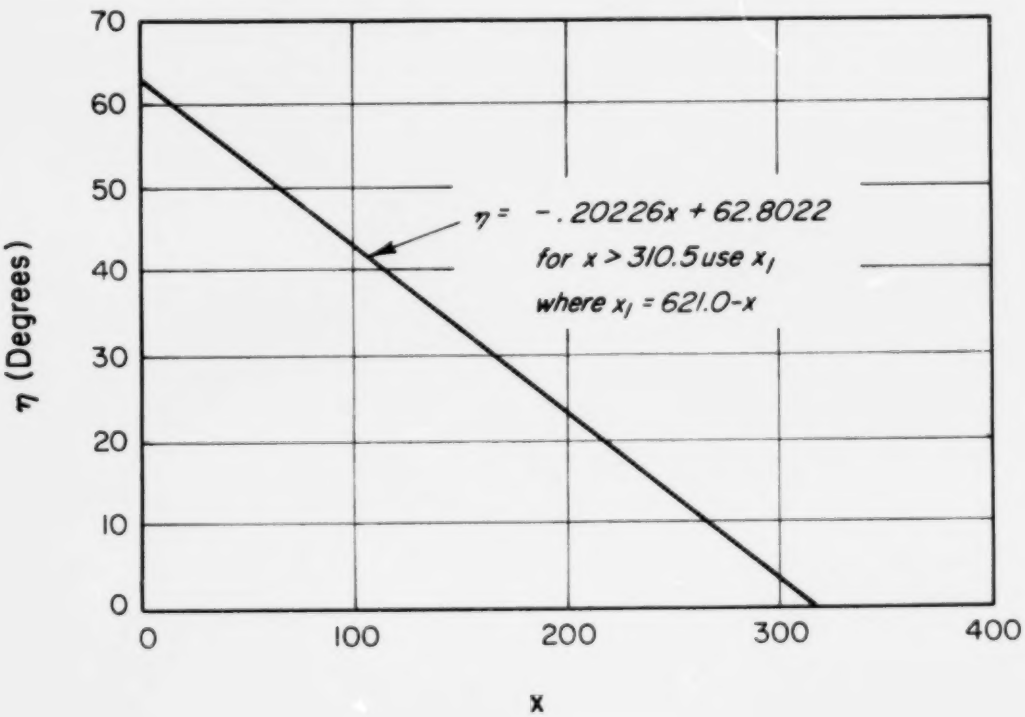

Figure 2.6b Graph of equation relating nadir angle (η) to scan spot number (x) along a scan line.

In order to compute the nadir angle of any scan spot along a scan line, the following linear equation was developed:

$$\eta = -.20226\ X + 62.8022$$

where X is the scan spot number (see Figure 2.6b). For $X > 310.5$, X_1 was used in place of X, where $X_1 = 621-X$.

The third program is depicted in Figure 2.7 in the form of a flow chart. Card input to the program consisted of maximum (CT_{max}) and minimum (CT_{min}) temperatures derived from climatological data for the chosen area, values of the deficit (D) computed from sounding information within the area of interest, an averaging interval into which the data is to be mapped, and a temperature correction, if any, for systematic bias (see Sections 3 and 5.6).

The program reads a scan line of infrared temperatures and the corresponding scan line of compressed visible data. Computation proceeds to where J is set equal to the number of the infrared scan spot in sequence and the corresponding compressed visible scan spot of brightness value (b) is tested for clouds in the field of view. Where $b \geq 8$ (see Section 4), it is assumed that clouds are present, and therefore, the infrared temperature for the observed spot is ignored and the test procedure is applied to the next one. When b_j is less than 8, the infrared value is tested to see if it is within the climatological temperature limits specified by CT_{min} and CT_{max}. If the T_B is accepted, a temperature correction is added and a test for use of a zenith angle correction is made. If the zenith angle correction is requested, z is computed to produce ΔT which is added to T_s, otherwise z is set equal to zero causing ΔT to become D. ΔT and D are corrections for atmospheric attenuation (see Section 5). When all scan lines have been processed, the mean temperatures are output in map form together with the corresponding population map of 'good' individual values of T_s used to compute each mapped value.

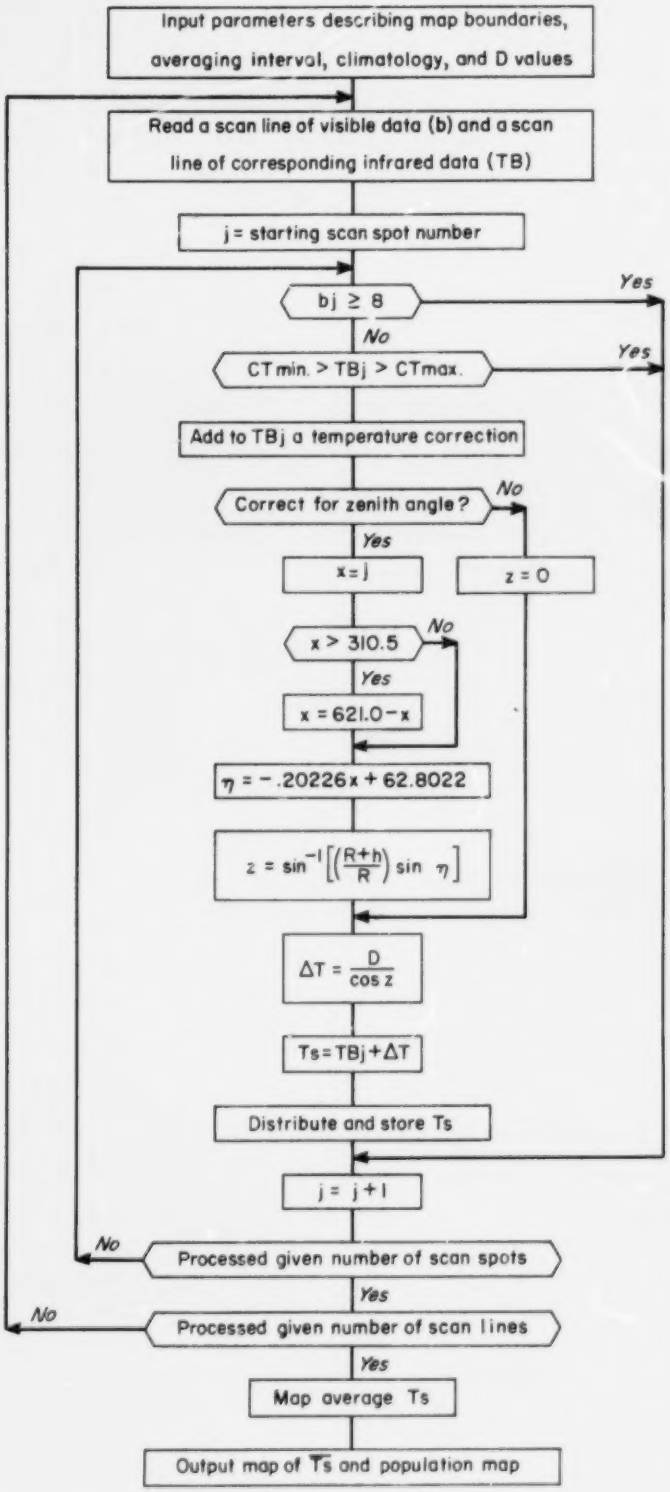
Input parameters describing map boundaries, averaging interval, climatology, and D values
Read a scan line of visible data (b) and a scan line of corresponding infrared data (TB)
j = starting scan spot number
bj ≥ 8
Yes
No
CT min. > TBj > CTmax.
Yes
Add to TBj a temperature correction
Correct for zenith angle?
No
Yes
x = j
z = 0
x > 310.5
No
Yes
x = 621.0 − x
η = −.20226x + 62.8022
z = sin⁻¹[((R+h)/R) sin η]
ΔT = D/cos z
Ts = TBj + ΔT
Distribute and store Ts
j = j + 1
No
Processed given number of scan spots
Yes
No
Processed given number of scan lines
Yes
Map average Ts
Output map of Ts and population map

Figure 2.7 Flow Chart of the Program for Mapping Sea Surface Temperature

3. SOURCES OF ERROR

Systematic or random errors in satellite data may arise from atmospheric effects, instrumental defects, or data processing procedures. Some more important sources of error for direct readout infrared data from the DMSP radiometer are the following:

1) Analog to digital conversion

2) Atmospheric attenuation
   a) cloud in the IFOV
   b) absorption by atmospheric gases, aerosols, and water vapor

3) Earth location

4) Signal noise

5) Calibration procedures
   a) electronic
   b) thermal

In a comparison of satellite data with ship measurements of sea surface temperature (T_S) additional sources of error may appear such as those of 'skin' effects and errors in the ship measurements.

The problem of atmospheric attenuation, which may be treated as an error in the context of inferring sea surface temperature, and some methods of accounting for it are discussed in Section 5 of this report. It has been assumed that no significant systematic error is present as a consequence of analog to digital conversion. Possible random error from that source is indistinguisable from signal noise in the data. Signal noise as well as some other sources of error are discussed in greater detail below.

3.1 Earth Location

Earth location includes gridding and the transfer of ship positions that were manually plotted on the infrared imagery to the digitized map of T_B. The geographical locations of the ships were supplied by FPRF.

A grid overlay was prepared for the imagery using the coordinates of various landmarks observable in the infrared and visible. The coordinates appeared accurate to within 1/2° of latitude; an error of 0.2 or 0.3° was most likely.

The transfer of ship positions from imagery to map was accomplished by comparing well defined cloud features. The accuracy of this procedure is within several tenths of a degree of latitude. Assuming the maximum deviation for both gridding and transfer of positions, the ship location on the map of T_B may differ from the recorded position by as much as 80 or 90 km. However, the MODE area is a region of relatively little spatial change in T_s. A review of ship measurements of T_s for the same time and an analysis of T_B indicate that the change in T_s over a distance of < 100 km is almost always < 1/2°K (see also Cogan and Willand, 1974).

3.2 Calibration Procedures

A number of factors in the calibration of the scanning radiometer system may introduce errors into the output of T_B. The calibration may be divided into two parts, electronic and thermal. Electronic calibration involves the conversion of analog voltage to digital count, and thermal calibration accounts for changes in the sensor caused by variation in temperature of the satellite.

Table 3.1 gives examples of calibration errors, their likely magnitude if known, and possible corrective actions. Information on these errors came from several private communications with EPRF and Westinghouse Electric Co. (builder of the DMSP radiometer) personnel during 1974-1975, and Spangler (1974).

Another factor that applies to calibration error arises as a consequence of the use of a "look-up" table to convert radiation to T_B. A range of radiation values are input into each category of T_B. The mean values of T_B used to represent the categories of T_B differ from each other by 1.7 or 1.8°K. Therefore an uncertainty of that size exists for any one "measurement" of T_B.

As best as could be determined with the available data, systematic bias may be as high as 5°K depending mostly on errors 2-6 of Table 3-1. (See also section 5.6).

TABLE 3.1

SOME ERRORS IN CALIBRATION

Source	Estimated Size	Corrective Action
1) Wow and flutter introduced into the data stream for scan angle information.	Unknown but will increase toward edges of earth view.	Correction Algorithm developed at EPRF
2) Shaping network to linearize temperature distribution from 210 to 310°K. 3) On board "black body source" not perfect. 4) Thermistor error for "black body source". 5) Spectral distortion of filter. 6) Assumed linearity of voltage to radiance curve.	The sum of 2-6 may cause an error of up to 5°K in absolute accuracy over the temperature range of interest. This error may vary with temperature.	Inspection of data for same area for different days and zenith angles where T_S does not change significantly (e.g. < 1/2°K) over the area of interest. Also comparison of observed and computed values of D. This latter method may be misleading since the calculated D may be incorrect by 1 or 2°K.

3.3 'Skin' Effect and Accuracy of Ship Measurements

The radiating surface ('skin') of the ocean may extend down only 25 or 50 μm for infrared radiation, while the layer of 'bulk' temperature generally refers to depths of about 10 cm (bucket temperature) to > 100 cm (in-take temperature). At night the skin temperature may be 1/2 to 1 1/2°C cooler than the bulk temperature as a consequence of radiational cooling (Ewing and McAlister, 1960; McAlister and McLeish, 1969). McAlister and McLeish also assume a similar effect during the day because only about 10% of incoming solar energy is absorbed in the top 0.5 mm. However, it is likely that on a calm or nearly calm sunny day the upper few centimeters would warm by as much as 1 or 2°C above the temperature of the water immediately below, causing a possible net warming of the 'skin' relative to the temperature of the bulk ($\geq$ 100 cm) layer. This supposition is supported by the work of Hanson and Poindexter (1972) and Bruce and Firing (1974) wherein they noted a warming of the upper two meters by 1.5 to 3°K in 12 hours (one 'day').

For this report the net difference between the surface and 'bulk' temperature has been assumed to be insignificant (no more than $\pm$ 0.1 or 0.2°K); the cooling of the top 50 μm relative to the water immediately below is roughly balanced by the warming of the top few cm (only values of T_B for apparently cloud-free IFOV's were used). This assumption would appear to be generally valid for the selected days, especially since no significant systematic bias was found in the satellite data.

In evaluating the satellite derived sea surface temperature it was assumed that the ship measurements of T_s were accurate. However, under the best conditions errors of at least several tenths of a degree are likely for bucket values. Such errors are likely to be larger for intake values of T_s, about 1°K or more. In conversations with personnel at Woods Hole Oceanographic Institute, ONR, and EPRF, it was indicated that the measurements for the MODE project were made by the bucket method, thereby minimizing the possible errors in T_s to about 0.5K. Comparison of ship measurements (297.8 to 298.2°K) with the one aircraft radiometric measurement (298.1°K) for 11 June suggest that these errors were somewhat smaller.

3.4 Emissivity of the Sea Surface

It has been assumed that the emissivity (ε) of the sea surface equals one for the inference of sea surface temperature from satellite measurements of infrared radiation in the atmospheric 'windows'. However ε of the sea surface varies with wavelength and viewing angle. Buettner and Kern (1965) measured the emissivity of a water surface at several wavelengths and found that $\varepsilon \approx 0.99$ for radiation near 10 or 11 μm where the angle of inclination (measured from the vertical) was less than about 48°. For an angle of about 56° ε was about 0.98 and decreased rapidly for greater angles. The above inclination (or zenith) angles are approximately equivalent to nadir angles of about 41° and 47° respectively. However, at wavelengths near 8 and 12.5 μm the emissivity departure from 1.00 is about twice that for 11 μm (e.g. 0.04 at 56° instead of 0.02). Therefore, for the 8-13 μm window the emissivity is probably about 0.985 for zenith angles < 48° and about 0.97 for an angle of 56°.

The above measurements were performed in a laboratory and, therefore, only serve to indicate the actual emissivity of the real ocean which may vary for different weather conditions. Nevertheless recent work with mapping of sea surface temperature (Cogan and Willand, 1974) using data from the NOAA-2 scanning radiometer suggests the validity of the assumption that $\varepsilon \approx 1.0$ for the sea surface at lower nadir angles (<40°). In any case, for $\varepsilon \geq 0.985$ the assumption of $\varepsilon = 1.0$ for the ocean would only result in an error of ≤ 0.5°K. The results presented in Figure 3.1 show the likely variations in computed sea surface temperature caused by possible deviations of ε from 1.0.

3.5 Signal Noise and Random Error

A measure of the variation of T_B caused by noise or random error within a given sample of data is the Root Mean Square (RMS) of the differences between individual values and the mean, sometimes called the RMS error (RMSE). A number of 10 x 10 scan spot "boxes", and one 10 x 14 "box", were selected for the three days to determine RMSE for each box, each day, and the whole three day period for the range of temperatures ($285.0 < T_B < 299.0$°K) assumed to represent cloud-free views

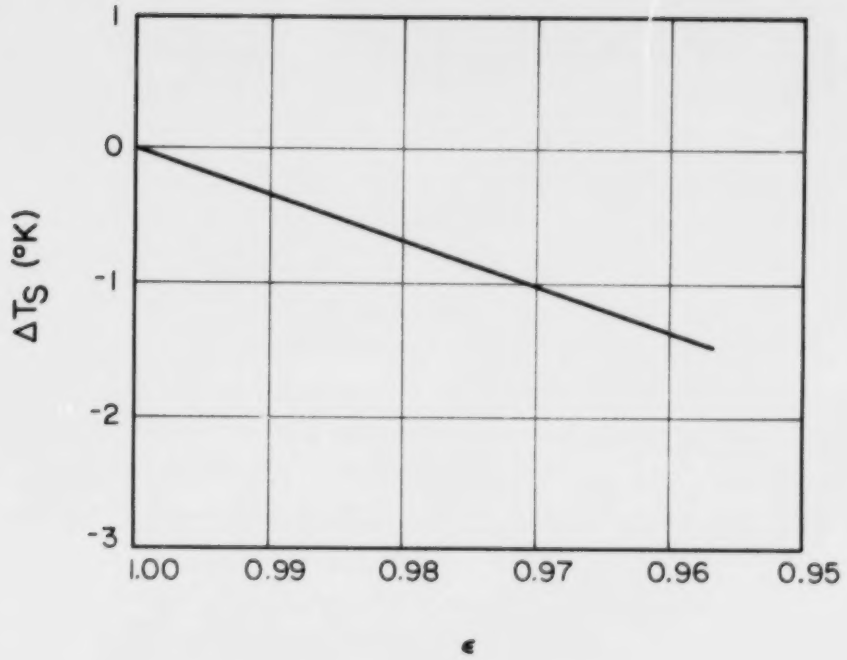

Figure 3.1 Apparent decrease in sea surface temperature (T_s) arising when the emissivity (ε) of the sea surface is not equal to 1.00. These apparent decreases were computed for a radiometer viewing the surface vertically through a typical Mid-Latitude summer atmosphere (Table 5.1).

and not to exceed T_s by more than about 1°K. The overall RMSE (three day value) was 0.92°K. Table 3.2 summarizes the results; the RMSE and sample size (i.e. number of 'good' values of T_B within each box) are given for each case. "Daily" values are also presented.

The RMSE values of Table 3.2 include random error from all satellite sources, suggesting that the contribution from any one component is generally small. Nevertheless total random error for any single measurement is likely to be about ±1°K. To assess the likely accuracy of a single measurement the uncertainty arising from the large size of the T_B categories must be taken into account (see Section 3.2). Combining both "errors" it is found that a likely accuracy for one value is only about ±1.8°K, not including atmospheric attenuation or systematic bias (uncertainty about mean $T_B \sim \pm 0.9$ and RMSE $\simeq \pm 0.9$).

An accurate (<±0.5°K) mean value of T_B, excluding any systematic bias, requires that a number of 'good' values be averaged to minimize noise. Williamson (1970) suggested a number ≥ 10 for HRIR (Nimbus 2) data and Cogan and Willand (1974) found that ≥ 6 values were sufficient for scanning radiometer (NOAA-2) data. However, as a consequence of the large inherent uncertainty in the data arising from the size of the T_B categories an accuracy of ±0.9°K appears to be the best that can be achieved even if systemic error is accounted for. Experience suggests that at least 5 values should be averaged to obtain even that accuracy (see, however, Section 6.3); under certain special conditions a greater accuracy may be possible. For example, if out of 100 scan spots 50 had a value of 288.6°K and the rest 290.3°K in a random distribution the "actual" T_B may be very close to the average of the two temperatures, say, 289.5 ±0.1°K. Therefore, the inaccuracy in the representative value of T_B for that box of scan spots caused by noise error would only be ±0.1°K.

TABLE 3.2

Values of RMS error for 21 'boxes' of scan spots. N gives the sample size for the corresponding RMS error (RMSE).

Date	'Daily' RMSE (°K)	'Daily' N	Case Number	RMSE	N
13 June 1973	0.91	587	1	1.37	96
			2	1.36	95
			3	1.19	96
			4	0.51	100
			5	0.51	100
			6	0.56	100
14 June 1973	0.80	750	1	0.62	100
			2	0.85	100
			3	0.99	94
			4	0.85	85
			5	0.75	100
			6	0.91	71
			7	0.91	100
			8	0.54	100
15 June 1973	1.07	655	1	1.31	67
			2	1.39	56
			3	1.07	140
			4	1.25	92
			5	0.97	100
			6	0.76	100
			7	0.99	100

4. THE CLOUD PROBLEM

Clouds within the instantaneous field-of-view (IFOV) will cause the temperature measured by the radiometer to be lower than for a cloud-free IFOV according to the amount and height of the intervening cloud. A very low equivalent black body temperature (T_B) of, say, 260°K or less over the ocean indicates the presence of middle, or high level, thick cloud covering all or most of the IFOV. Therefore broken or overcast middle or high clouds, except thin cirrus, are easily detected by the infrared radiometer.

However, an IFOV containing either a few widely scattered clouds, very thin cirrus, a very low cloud layer, or fog may be indistinguishable from a cloud-free IFOV because T_B would be lowered only slightly. The general higher reflectivity of cloud compared with the sea surface enables a view of a low cloud layer or fog to be distinguished from one of a cloud-free area through the use of data from a sensor operating in the visible portion of the spectrum. Scattered clouds which are not too small may be observed by the visible sensor of the DMSP radiometer because of its greater resolution compared with that of the infrared sensor. The IFOV of the DMSP radiometer, infrared channel, is, unfortunately, too large (4.3 km along the sub-satellite track) for the detection of scattered low cumulus or strato-cumulus, especially those of a diameter of, say, $\leq$ 0.5 km. The visible sensor (0.6 km) should be able to detect the smaller clouds but the resolution was degraded to only slightly less than that of the infrared (3.1 to 3.7 km) in order to reduce data processing (see Section 2). Therefore, even by using both infrared and visible data only 'larger' clouds or groups of cloud are detectable; the likely cooling of T_B would only be about 1 or 2°K for small widely scattered Cu or Sc making them virtually impossible to detect. The elimination of scan spots which may only be partially filled with scattered low clouds must be accomplished through other techniques. Furthermore, a thin layer of cirrus which is not observed in the visible may have a significant effect on the infrared data, causing a possible lowering of T_B of > 2°K (see also Rao, 1975).

Some apparent relationships between the visible and infrared data, possible sources of inconsistencies in those relationships, and methods

of delineating significant cloud regions will be discussed in the rest of this section.

4.1 Relationship Between Visible Brightness and Radiance Temperature

A cloud layer can be expected to cause a decrease in the T_B inferred from infrared radiances measured by a satellite and an increase in the corresponding visible brightness value (b). This effect would be particularly noticeable for a thick cloud with a top at middle or high levels which filled the entire IFOV. Several "threshold" values of brightness were found that approximately delineate various categories of cloud amount and T_B. The magnitude and gross significance of these threshold b's are summarized in Table 4.1. The relationship between b and T_B were established through comparison between corresponding maps of these values. The cloud cover information is based on interpretation of the imagery data. These threshold values will change with latitude and time of day as a result of different zenith angles of the sun.

A number of inconsistencies were noticed when comparing the maps of b with the corresponding maps of T_B. Although areas of high b and low T_B for large cloud regions approximately coincide, smaller areas were often displaced relative to one another. Furthermore, a single or small group (2 or 3 scan spots) of high b may not have a corresponding low T_B. These and other less obvious differences may be a consequence of one or more of the factors listed below:

1) Sun glint
2) Fog or very low stratus
3) Very thin cirrus
4) Cloud shadow on another cloud
5) Greater resolution of averaged data from visible sensor
6) Noise

Natural phenomena in the above list were noticed in the DMSP data. Factors (2) and (3) may cause a similar decrease in the observed T_B, but may show up differently in the visible. Scattered small Cu or Sc detected in the visible may be missed in the infrared on account of (5).

TABLE 4.1

Brightness value, b (digital counts)	Cloud amount and T_B (°K)
$b \geq 10$	Almost always cloud and lower values of T_B.
	Generally overcast or broken cloud cover. Some exceptions noted. $T_B < 285$
$9 \geq b \geq 6$	Generally partial cloudiness.
	Relationship unclear. Many exceptions. $T_B \sim 282$ to 289
$5 \geq b$	Generally cloud-free conditions and higher values of T_B
	Few exceptions. $T_B > 287$

Approximate relationships between b and cloud amount or T_B. No visible brightness value less than 5 was observed. For the intermediate category, $9 \geq b \geq 6$, there was a rough increase in the proportion of "cloudy" scan spots as b increased. The relationship between b and T_B is only a rough estimate since no clear relationship was apparent.

Isolated anomalous b's or T_B's may be a consequence of noise as may be occasional lines of anomalous data parallel or perpendicular to the sub-satellite track. Sun glint appears as a region of high b associated with an area of high T_B. Martin and Scherer (1973) also discuss the problem of the lack of consistent agreement between co-located centers of high b and low T_B, but for NOAA-1 data.

4.2 Delineation of Cloud

Large cloud regions may be isolated on both visible and infrared data maps. Cloud is almost always present where $b \geq 10$ digital counts (see Table 4.1). An analysis of each map of visible data for $b \geq 10$ usually separates cloud-filled from mostly cloud-free regions. However, several of the factors listed above, such as sun glint, can lead to an erroneous analysis of the cloud field. Individual or small groups of high b may not indicate the presence of a cloud or may place it incorrectly relative to its position on the corresponding map of T_B. Therefore, a map of b alone cannot delineate the entire cloud field, but must be used in conjunction with the corresponding map of T_B (see also Rao, 1975).

On maps of T_B the 281°K isotherm almost always delineated large cloud covered regions in the MODE area for 13 through 15 June 1973. Furthermore, any T_B less than about 286°K usually indicated cloud in the IFOV based on the work used to derive Table 4.1 and climatological data. Higher values of T_B could still partially be a measurement of the radiance temperature of small scattered clouds, thin cirrus, warm near-surface stratus, or fog. Information from the maps of b can help to delineate areas containing near-surface stratus or fog, but may not be of use for thin cirrus or small scattered clouds (see also above).

Each type of data (visible or infrared) cannot be used by itself to obtain a complete picture of the cloud field, but by a careful comparison of b with T_B maps of the same area most cloud contaminated IFOV's can be eliminated. Nevertheless, very thin cirrus or widely scattered small Cu or Sc may escape detection by both the visible and infrared components of the DMSP radiometer. By a suitable technique for averaging those values of T_B for apparently cloud-free scan spots, the problem

of the aforementioned cloud situations can be appreciably diminished. Such a scheme will be discussed in following sections (5 and 6) on the computation of the temperature deficit (D) and T_s.

5. THE DEFICIT, A CORRECTION FOR ATMOSPHERIC ATTENUATION

Several algorithms were developed for the computation of the likely attenuation of upward radiation from the sea surface in the so-called 8-13 μm 'window'. A convenient measure of the attenuation is the difference between the sea surface temperature and the equivalent black body temperature of the radiation measured by a radiometer looking vertically through a cloud-free atmosphere, herein called the deficit.

The DMSP radiometer responds to radiation between about 7.7 and 13.15 μm (about 760 to 1300 cm^{-1}) and most strongly to radiation between 8 and 13 μm (about 770 to 1250 cm^{-1}). Within this broad spectral region radiation is attenuated most significantly by water vapor (lines and continuum), ozone, carbon dioxide, and aerosols. Following brief discussions on these atmospheric constituents and the atmospheric models used, the computer algorithm for computing the deficit is outlined. Values of total water vapor content computed with radiosonde data are compared with estimates derived from satellite measurements. Methods of estimating the deficit with and without concurrent measurements of atmospheric variables are discussed and their accuracy assessed. Finally, observed deficits are compared with computed values.

5.1 Primary Absorbers and Model Atmospheres

The most significant atmospheric attenuators are water vapor, ozone, carbon dioxide, aerosols, and to a lesser extent CH_4 and N_2O at wavelengths below about 8.2 μm. The water vapor continuum extends throughout the interval from 7.7 to 13.15 μm commonly referred to as the 8-13 μm interval or window, and the strong water vapor band centered near 6.7 μm attenuates at the lower wavelength (higher wave number) side of the window. The resultant attenuation or deficit of temperature, in terms of °K per atmosphere, varies greatly with water vapor amount and distribution from less than 0.5°K atm^{-1} for a dry polar atmosphere to greater than 5°K atm^{-1} for a moist tropical atmosphere.

The strong ozone band centered near 9.6 μm lies entirely within the 8-13 μm window and, furthermore, the relative spectral response of the DMSP radiometer is at its maximum near 9.6 μm. Consequently, absorption by ozone contributes a large part to the total deficit which will differ for changing distribution and/or total content. Total ozone in cm-atm varies in an opposite latitudinal sense from total water vapor in that it generally decreases from about 0.480 cm-atm for a winter polar atmosphere to about 0.250 cm-atm for a tropical atmosphere (McClatchey et al, 1972 and Wu, 1973 and 1974). The distribution of ozone also changes in both space and time, but profile measurements are scarce and, consequently, only climatological and scattered daily values are available for a relatively few stations (see also DÜtsch, 1974). A typical value of the deficit arising from absorption by ozone is about 4 to 5°K atm^{-1}.

Aerosols vary considerably, spatially and temporally, but good estimates of the part of the total deficit resulting from aerosol extinction (absorption and scattering) may be obtained through the use of a representative distribution of particle size and number density with height, (e.g., Deirmendjian, 1964). Number density profiles may be constructed for a 'hazy' or a 'clear' atmosphere while using the same distribution of particle size (McClatchey et al, 1972). In general, extinction by aerosols generally contributes less than 1°K atm^{-1} to the total deficit.

Carbon dioxide and other so-called 'uniformly mixed gases' (McClatchey, et al) such as, for example, CH_4 vary only slightly from place to place and may, therefore, be treated as having a constant mixing ratio. Carbon dioxide varies only slowly with time and the other gases cause only a relatively small amount of attenuation in the 8-13 μm interval. The contribution to the deficit arising from absorption by carbon dioxide and the other 'uniformly mixed gases' may be about 1°K atm^{-1}.

The above crude estimates of the deficit caused by each atmospheric constituent were obtained by applying the data presented in McClatchey et al, to representative atmospheres. Figure 5.1 shows computed attenuation for a Mid-latitude atmosphere in terms of the deficit for the spectral interval of the DMSP radiometer at a spectral resolution of

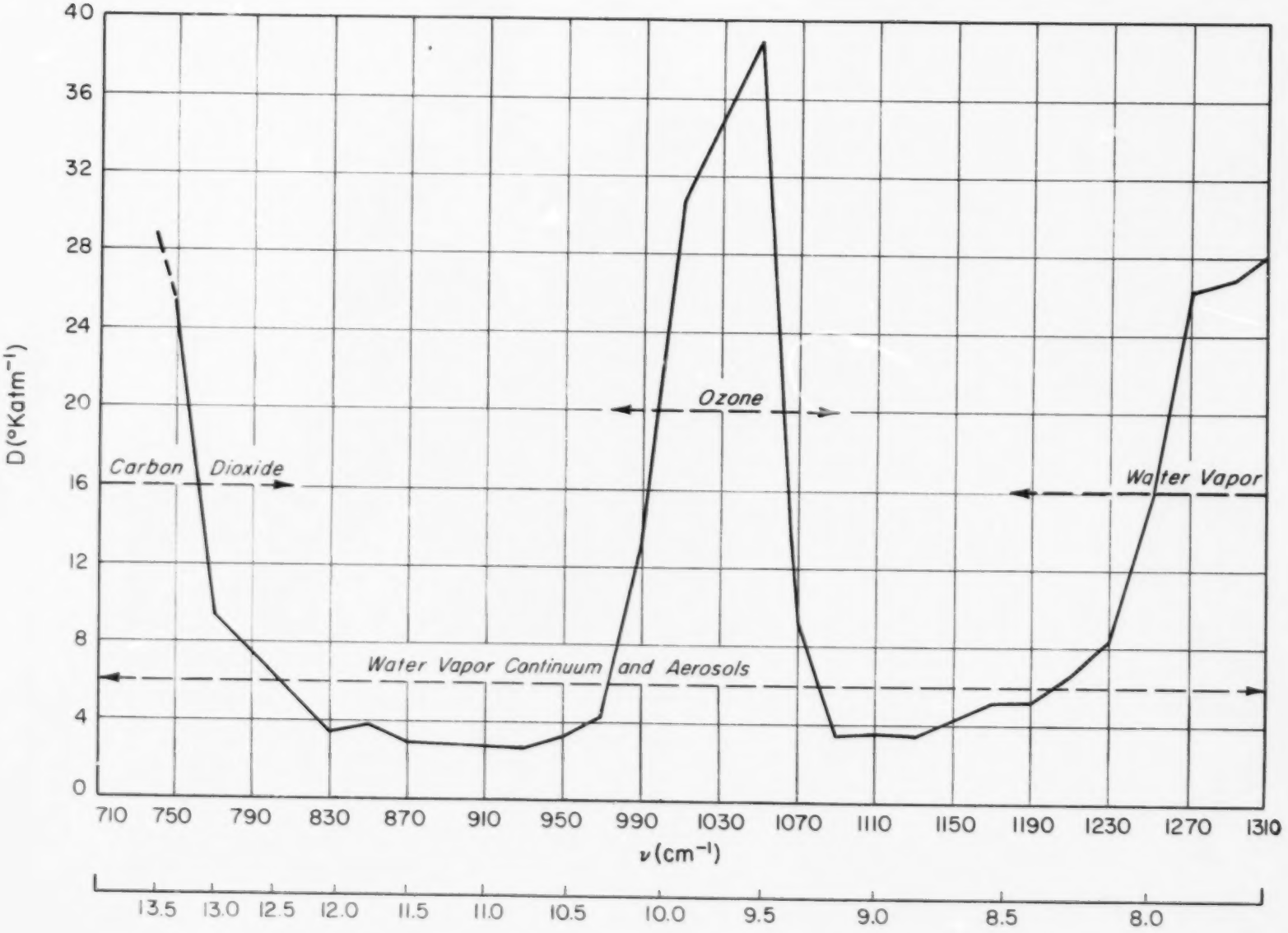

Figure 5.1 Values of the deficit (D) for intervals of 20 cm^{-1} and approximate spectral range of the primary attenuators. Values of D were computed for a unit bandpass radiometer.

9362

20 cm^{-1}. Values of the deficit were calculated with the computer algorithm (Section 5.2) based on the LOWTRAN-2 program developed at AFCRL (McClatchey et al, and Selby and McClatchey, 1972). Approximate regions affected by each absorber are also indicated.

Values of meteorological parameters used for the computation of the deficit were derived from a combination of actual measurements and climatological values for 1 km levels from the surface through 25 km, and for various levels up to 100 km. Radiosonde soundings launched from Ship HUNT on 13, 14 and 15 June 1973 provided measurements of temperature (T), pressure (p), and dew point depression (ΔT_d) for heights up to about 4 km. Water vapor density (ρ_v) was computed from T, p, and ΔT_d assuming hydrostatic conditions. Climatological values of T, p, and ρ_v were extracted from the Mid-latitude Summer model atmosphere (Table 5.1) given by McClatchey et al (1972) for heights $\geq$ 7 km. Estimates of T, P, and ρ_v for intermediate levels (i.e., 5 and 6 km) were extrapolated from the last sounding measurement and adjusted in accordance with values from Table 5.1 to avoid discontinuities.

McClatchey et. al. supplied the ozone profile used in the computer program (see Table 5.1). This profile was chosen because the total ozone content closely approached Dobson measurements of total ozone at Tallahassee for late June 1973 and climatological values for the MODE area in June (see Dütsch, 1974 and Wu, 1973). Note that densities (ρ) shown in the Table were computed from the listed pressures, temperatures, and vapor densities, and therefore, values of ρ used in the computations for heights less than 7 km were different from those shown.

5.2 Computation of the Deficit

The basis of the algorithm for computing the deficit is the LOWTRAN-2 program developed at AFCRL (See Selby and McClatchey, 1972 and McClatchey et al, 1972). LOWTRAN-2 computes the transmission from a given level to space at various spectral resolutions (for this study the smallest, 20 cm^{-1}, was used) for any spectral interval between 0.25 and 28.5 μm (40,000 to about 350 cm^{-1}). In this study, computations were made for the spectral interval of the DMSP radiometer, from about 760 to 1300 cm^{-1}.

Each atmosphere is divided into 33 homogeneous layers where the layer value of an atmospheric parameter (e.g., temperature, vapor density,

TABLE 5.1
MODEL ATMOSPHERE USED AS A BASIS OF THE COMPUTATION OF ATMOSPHERIC OPTICAL PROPERTIES

(from McClatchey et al, 1972)
MID-LATITUDE SUMMER

Ht. (km)	Pressure (mb)	Temp. (°K)	Density (g/m^3)	Water Vapor (g/m^3)	Ozone (g/m^3)
0	1.013E+03	294.0	1.191E+03	1.4E+01	6.0E-05
1	9.020E+02	290.0	1.080E+03	9.3E+00	6.0E-05
2	8.020E+02	285.0	9.757E+02	5.9E+00	6.0E-05
3	7.100E+02	279.0	8.846E+02	3.3E+00	6.2E-05
4	6.280E+02	273.0	7.998E+02	1.9E+00	6.4E-05
5	5.540E+02	267.0	7.211E+02	1.0E+00	6.6E-05
6	4.870E+02	261.0	6.487E+02	6.1E-01	6.9E-05
7	4.260E+02	255.0	5.830E+02	3.7E-01	7.5E-05
8	3.720E+02	248.0	5.225E+02	2.1E-01	7.9E-05
9	3.240E+02	242.0	4.669E+02	1.2E-01	8.6E-05
10	2.810E+02	235.0	4.159E+02	6.4E-02	9.0E-05
11	2.430E+02	229.0	3.693E+02	2.2E-02	1.1E-04
12	2.090E+02	222.0	3.269E+02	6.0E-03	1.2E-04
13	1.790E+02	216.0	2.882E+02	1.8E-03	1.5E-04
14	1.530E+02	216.0	2.464E+02	1.0E-03	1.8E-04
15	1.300E+02	216.0	2.104E+02	7.6E-04	1.9E-04
16	1.110E+02	216.0	1.797E+02	6.4E-04	2.1E-04
17	9.500E+01	216.0	1.535E+02	5.6E-04	2.4E-04
18	8.120E+01	216.0	1.305E+02	5.0E-04	2.8E-04
19	6.950E+01	217.0	1.110E+02	4.9E-04	3.2E-04
20	5.940E+01	218.0	9.453E+01	4.5E-04	3.4E-04
21	5.100E+01	219.0	8.056E+01	5.1E-04	3.6E-04
22	4.370E+01	220.0	6.872E+01	5.1E-04	3.6E-04
23	3.760E+01	222.0	5.867E+01	5.4E-04	3.4E-04
24	3.220E+01	223.0	5.014E+01	6.0E-04	3.2E-04
25	2.770E+01	224.0	4.228E+01	6.7E-04	3.0E-04
30	1.320E+01	234.0	1.322E+01	3.6E-04	2.0E-04
35	6.520E+01	245.0	6.519E+00	1.1E-04	9.2E-05
40	3.330E+00	258.0	3.330E+00	4.3E-05	4.1E-05
45	1.760E+00	270.0	1.757E+00	1.9E-05	1.3E-05
50	9.510E+01	276.0	9.512E-01	6.3E-06	4.3E-06
70	6.710E-02	218.0	6.706E-02	1.4E-07	8.6E-08
100	3.000E-04	210.0	5.000E-04	1.0E-09	4.3E-11

Total atmospheric content Water Vapor: 2.98 g cm^{-2}

Ozone: 0.324 atm cm (0.695×10^{-3} g cm^{-2})

etc.) is the average of the values at the two boundary levels (see Table 5.1). The Planck function (B) is computed for every layer and the surface (B_s) at the mean wave number of each 20 cm^{-1} interval (i.e., 770, 790,...1290 cm^{-1}).

To compute the radiance from the surface to space for a transmission τ_s from the surface we have:

$$R_s = B_s \tau_s$$

and from each level:

$$R_m = B_m \tau_m$$

The radiation from each layer is the radiation reaching space from the upper boundary (upper adjacent level) less that from the lower boundary. Therefore, for the computation of the contribution from each of the 33 layers to the net radiance reaching space we have:

$$R_n = B_n \times (\tau_{m+1} - \tau_m)$$

where n represents a given layer and m a given level. This equation may be verified by referring to a simple radiation diagram representing 3 or 4 layers where τ is the abscissa and B the ordinate. The individual contributions are summed over N (=33) layers and added to the surface contribution to obtain the aperture radiance

$$R = R_s + \sum_{n=1}^{N} R_n$$

From the curves of spectral response for the DMSP sensor supplied by Westinghouse (private communication) we may derive a filter function, $f(\phi)$, which is the sum of the mean spectral responses for the 20 cm^{-1} intervals.

$$f(\phi) = \sum_{m=1}^{M} \phi_m \Delta\nu$$

where m represents the mean value for each interval and $\Delta\nu$ = 20 cm^{-1}

The weighted mean radiance ($\overline{R}$) and wave number ($\overline{\nu}$) are computed for the broadband DMSP radiometer according to the following equations:

$$\overline{R} = \frac{\int_{\nu_1}^{\nu_2} R_\nu \phi_\nu d\nu}{\int_{\nu_1}^{\nu_2} \phi_\nu d\nu} \simeq \frac{\sum_{m=1}^{M} \Delta\nu \, R_m \phi_m}{\sum_{m=1}^{M} \Delta\nu \, \phi_m}$$

and

$$\overline{\nu} = \frac{\int_{\nu_1}^{\nu_2} \nu \phi_\nu d\nu}{\int_{\nu_1}^{\nu_2} \phi_\nu d\nu} \simeq \frac{\sum_{m=1}^{M} \Delta\nu \, \nu_m \phi_m}{\sum_{m=1}^{M} \Delta\nu \, \phi_m}$$

where m represents the mean value for each interval of 20 cm^{-1}, and ν_1 and ν_2 are 760 and 1300 cm^{-1}. The approximate value of the equivalent black body temperature (T_B) for $\overline{R}$ is computed from the wave number form of the Planck equation for $\nu = \overline{\nu}$.

This approximate value becomes the initial guess for the determination of the 'best' value of T_B by an iterative technique. An iterative method is necessary because the above technique of 'mean wave number' is only accurate for relatively narrow spectral intervals where the absorption varies only relatively slowly with wave number (e.g. the infrared window radiation sensed by the scanning radiometer carried on the NOAA-2 satellite). The T_B computed with the 'mean wave number' method is only accurate to about 1 to 1.5°K for a typical summer atmosphere at middle latitudes for the DMSP broadband radiometer.

The iterative technique makes use of the following relationship:

$$\overline{R} = \int_{\nu_1}^{\nu_2} B_\nu \, (T_B) \, d\nu$$

and

$$\overline{R} \simeq \sum_{m=1}^{M} B_m (T_B) \Delta\nu$$

where m represents the mean value for each 20 cm^{-1} interval and B is the Planck function. It may also be shown that for radiation near 10 μm (1000 cm^{-1}) $B \alpha T_B^x$, where x is close to 5. The ratio of $\overline{R}$ and $\overline{B}$ ($\overline{B} = \sum_{m=1}^{M} B_m (T) \Delta\nu$) may be used to obtain a guess for the value of T_B.

$$\overline{R}/\overline{B} = (T_B/T)^5$$

$$T_B = T (\overline{R}/\overline{B})^{1/5} \qquad (2)$$

The iterative process proceeds as follows:

1) An initial 'guess' value, $\overline{B}$, is computed from the approximate value (T) of T_B.

2) $\overline{B}$ is compared with $\overline{R}$ by using the ratio $\overline{R}/\overline{B}$ and determining whether or not it varies from unity by more than ε, where ε = 0.001 for an accuracy in T of about 0.1°K relative to T_B. The size of ε can, of course, be changed if other accuracies are desired.

3) If the two quantities $\overline{R}$ and $\overline{B}$ are not sufficiently close a new T, or 'guess' value of T_B, is calculated with equation (2).

4) A new value of $\overline{B}$ is computed with the new T.

5) The procedure is repeated until $1.000-\varepsilon \leq \overline{R}/\overline{B} \leq 1.000 + \varepsilon$ as in Step 2 above.

6) T_B is assumed to equal the resultant value of T.

Once T_B has been calculated, it is subtracted from the sea surface temperature (T_S) in order to obtain the deficit (D); $D = T_s - T_B$.

5.3 A Parametric Formula

Computation of D by the aforementioned computer method may require a vast amount of computer time and expense if applied to the mapping of

T_s over an extensive area. Consequently, a parametric formula has been devised that gives an estimate of D in terms of total water vapor content (M) and total ozone content (U). Contributions to D from absorption by carbon dioxide and other "uniformly mixed gases" (see McClatchey et al, 1972) and by aerosol extinction are represented by constants to a sufficient accuracy.

The contribution (D_{wc}) arising from continum absorption by water vapor may be estimated by a variation of the formula devised by Cogan and Willand (1974), but for radiation at a mean wavenumber of 1024 cm^{-1} (wavelength, λ, of about 9.8 μm). It was assumed that the source function (J) is proportional to a power of the pressure (P) in atmospheres. $J = J_o P^{\ell}$ where $\ell = 0.9$ for radiation near 9.8 μm and J_o is the surface value. It was noted by Cogan and Willand that the mixing ratio (r_o) is also proportional to P; $r = r_o P^n$ where r_o is the surface value and n = 3 for typical tropospheric profiles. These values of ℓ and n are then substituted into the equation for D_W for a representative sea surface temperature (T_s).

$$D_W = \alpha\ (\lambda,\ n,\ \ell,\ T)\ k_1 M + \beta\ (\lambda,\ n,\ \ell,\ t)\ k_2 M^2$$

where $\alpha = 8.1$ and $\beta = 2.1$

For k_1 and $k_2 = 0.10$ and $5 g^{-1} cm^2$ (see Cogan, 1972) and substituting the above values of α and β the following is obtained:

$$D_{wc} = 0.81M + 0.105M^2 \qquad (3)$$

However, Eq (3) does not account for attenuation by water vapor lines; such absorption may be important in the 7.7 to 13.15 μm interval of the DMSP radiometer. Some simple calculations using output from the computer method suggest that additional attenuation from water vapor lines, i.e. not accounted for in (3), is generally less than $0.5°Katm^{-1}$ for the cases studied. Based on these calculations, a crude estimate of the contribution from absorption by water vapor lines may be computed by the expression $D_{w\ell} \sim 0.1M$. By including this expression with Eq (1), we have $D_w = D_{wc} + D_{w\ell}$ or:

$$D_w = 0.91\ M + 0.105M^2$$

D_w may be read off Figure 5.2 as a function of M for values commonly encountered in the atmosphere. For 8 of the 14 cases examined Eq (2) gave D_w to < 0.2° $Katm^{-1}$ of the computed value (D_{cw}) and < 0.8° $Katm^{-1}$ for all but one case. To compute D_{cw} the water vapor densities at all levels were multiplied by 10^{-8} which effectively eliminated water vapor from the model atmospheres. By subtracting the resultant deficit from the value (D_c) computed with water vapor we have D_{cw}. The accuracy of this technique is apparently ~ 0.1 to 0.2° $Katm^{-1}$.

The contribution (D_o) to the deficit arising from absorption by ozone may be approximated by a formula that gives D_o as a function of total ozone (U). The formula was derived by computing D_o for various values of U, whereby, for each U ozone densities at every level of the Midlatitude Summer atmosphere were multiplied by a constant, effectively causing a shift of the profile to higher or lower values (profile shape remained constant). The constants selected were 0.7, 0.8, ..., 1.2, and 1.3. Additionally, D_c was computed for the case of "no" ozone (constant = 10^{-8}) to obtain a base value from which values of D_o were calculated ($D_o = D_c - D_c$[without ozone]). Figure 5.3 shows values of D_o plotted against U for the Midlatitude Summer atmosphere. A straight line was fitted to the curve of D as a function of U that is good to ±0.1°$Katm^{-1}$ for values of $0.230 \leq U \leq 0.430$ cm atm. This line is given by:

$$D_o = 5.7U + 2.8 \text{ where } D_o \text{ in } ^\circ Katm^{-1} \text{ and U is in cm atm.} \qquad (4)$$

It is important to note that a new formula should be computed for each climatic region since the mean profile of ozone is not the same for all regions.

Computations of D_c without haze and with the two haze distributions (surface visibilities of 5 and 23 km) suggested that the contribution to D (D_a) from extinction by aerosols may have ranged from about 0.3 to 0.5° $Katm^{-1}$ for most atmospheres (see Table 5.2). A likely value for D_a was about 0.4 °$Katm^{-1}$ since most reported surface visibilities in the vicinity of the MODE area generally were about 8 to 23 km under cloud-free conditions. Further computations of D_c with water vapor and ozone removed indicated that the residual attenuation arising from

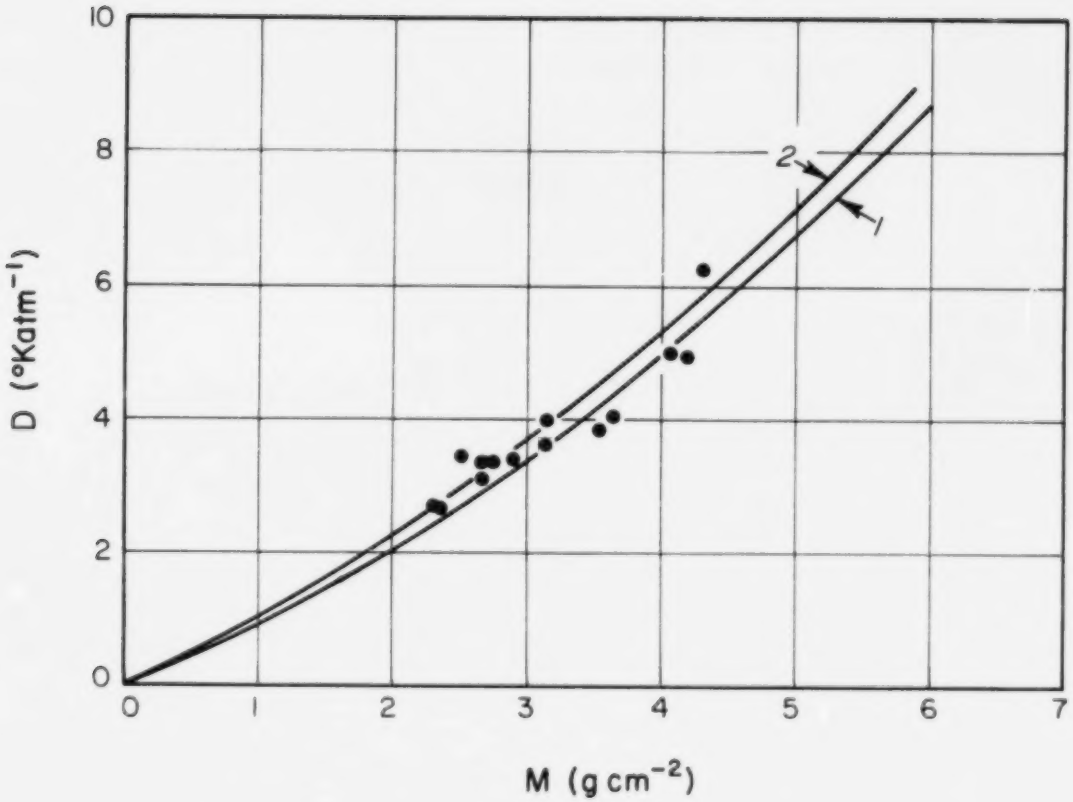

Figure 5.2 The deficit (D_w) arising from absorption by (1) water vapor continuum only (lower curve) and by (2) water vapor continuum plus lines (upper curve) computed by parametric formulas. D_w is plotted as a function of integrated water vapor (M). Values of D_w computed by numerical integration are plotted as circled points.

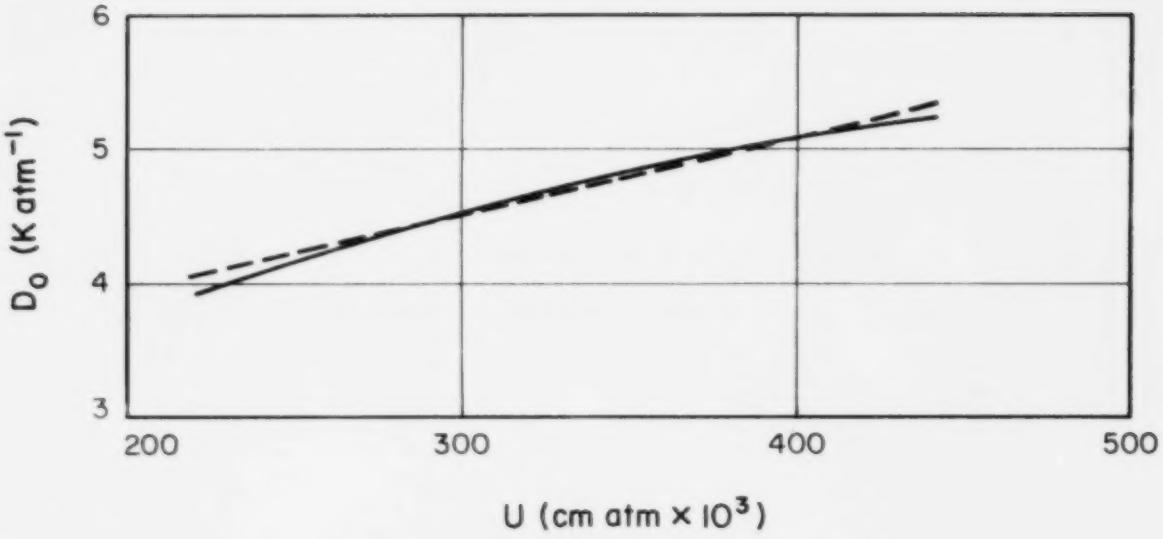

Figure 5.3 Values of the deficit (D) arising from ozone absorption computed for various values of total ozone content (U). Dashed line gives approximate values for $0.230 \leq U \leq 0.430$ cm atm. All curves were drawn for a typical Mid-Latitude Summer atmosphere.

the presence of aerosols, carbon dioxide and "uniformly mixed gases" produced a contribution of about 1.4° $Katm^{-1}$. Subtracting D_a from this residual value we have D_g (~ 1.0° $Katm^{-1}$), the contribution arising from absorption by carbon dioxide and "uniformly mixed gases."

The value of D may be roughly estimated by adding together the several components:

$$D_p = D_w + D_o + D_a + D_g$$

where D_p is the parametric value of D.

By substituting the corresponding expressions and constants:

$$D_p \approx 0.91M + 0.105\ M^2 + 5.7U + 2.8 + 0.4 + 1.0 \qquad (5)$$

TABLE 5.2

DEFICITS FOR VARIOUS HAZE DISTRIBUTIONS

Atmosphere	Haze Model		
	0	1	2
Midlatitude Summer	8.73	8.98	9.13
Tropical	10.30	10.57	10.74

0 = No haze or aerosols

1 = Haze such that surface visibility is 23 km

2 = Haze with surface visibility of 5 km.

Listed deficts are in °$Katm^{-1}$. The atmospheres were taken from McClatchey et al (1972). See also Table 5.1

However, in practice no daily measurements of U were made for the MODE area. Therefore, an appropriate mean value must be selected based on climatology and nearby (if any) day-to-day measurements. Tallahassee measurements (Dobson meter) for late June 1973 and climatological values from Wu (1973) and Dütsch (1974) suggest a mean value for U of about 0.320 cm atm. Since this value nearly coincides with the U (0.324 cm atm) computed from the mean profile for the Mid-latitude Summer atmosphere (see Table 5.1) this latter value of U and the corresponding profile were selected to be representative of the MODE region in June 1973. For U = 0.324 cm atm, $D_o \approx 4.65$ °$Katm^{-1}$ and Eq (5) may be written:

$$D_p \simeq 0.91\ M + 0.105\ M^2 + 6.05 \qquad (6)$$

Table 5.3 lists values of D computed by the computer method (D_c) and by the parametric formula (D_p). Values of D_w and M are also given in the table for each D_p and D_c. As can be seen from this table, the parametric formula for 13 of 14 cases estimates D to $< \pm 0.6°K\ atm^{-1}$ of the computer values for the MODE region in June. The one difference $> \pm 0.6°\ Katm^{-1}$ most likely occurs because of a large deviation of the atmospheric profiles of temperature and humidity from the assumed shapes used to derive Eq (3). Also attenuation by ozone is partially dependent on the difference between the average temperature of the maximum ozone layer (centered near 22 km) and the surface temperature. The "constant" for D_o was computed for a T_s of 294°K while T_s for the standard atmosphere was 304.6°K.

5.4 Measurement of Integrated Water Vapor by NEMS and Radiosonde

Sea surface temperature (T_s) may be derived entirely from satellite data provided that concurrent 'measurements' of M and T_B are available. A comparison between radiosonde and satellite derived values of M indicate that M may be estimated to $< 0.5\ g\ cm^{-2}$ (3 of 5 cases to $< 0.15\ g\ cm^{-2}$) of radiosonde values (Cogan and Willand, 1974). These results were obtained using data from the NEMS (Nimbus-E Microwave Radiometer) carried on the Nimbus 5 satellite for January 1973. Staelin et al, 1973 found that the 'error' in M is typically $< 0.4\ g\ cm^{-2}$ in a comparison of satellite with radiosonde values, and Salomonson (1974) noted that recent Nimbus 5 observations indicated that M may be estimated to within about ± 10% for many atmospheres. The Nimbus 5 User's Guide (1972) provides a description of the NEMS.

The deficit (D_w) arising from absorption by water vapor may be computed using the parametric formula without the additional 'constant' terms (see Eqs (4) and (6) above). Only D_w was computed since the summer ozone profile used in the derivation of Eq (5) may not be applicable for the winter. In any case, differences between values of D_w computed using values of M from NEMS and radiosonde would be the same as differences

TABLE 5-3

COMPARISON OF DEFICITS COMPUTED WITH THE PARAMETRIC EQUATION AND THE NUMERICAL INTEGRATION SCHEME

ALL VALUES OF D AND ΔD IN °K atm^{-1}; M in g cm^{-2}

Date and Time (Hr Day for June 1973)	M	D_w	D_P	D_c	ΔD (= $D_p - D_c$)
1209	2.680	3.19	9.24	9.68	- 0.44
1110	2.333	2.69	8.74	8.79	- 0.25
2310	2.624	3.11	9.15	9.37	- 0.22
1111	2.640	3.13	9.18	9.37	- 0.19
2311	2.496	2.93	8.98	8.98	0.30
1212	2.365	2.74	8.79	8.96	- 0.17
2312	2.659	3.16	9.21	9.80	- 0.59
1213	2.913	3.54	9.59	9.80	- 0.21
1214	4.194	5.66	11.71	11.44	0.27
2314	4.067	5.44	11.49	11.44	0.05
1215	3.539	4.54	10.59	10.20	0.39
2315	3.157	3.92	9.97	10.42	- 0.45
1216	3.647	4.72	10.77	10.45	0.32
Standard Atmosphere, July 30°N (to 7 km)	4.308	5.87	11.92	13.26	- 1.34

in D_p since ozone absorption would be treated as a constant for reasons given in section 5.3. The consequent difrerences were < 0.6°K atm^{-1}; < 0.2°K atm^{-1} for 3 of the 5 cases. Table 5.4, based partly on Table 5.3 of Cogan and Willand (1974), shows the results for all cases.

Estimates of T_s may be made to a useful accuracy using satellite data alone if a remote sounder at least as accurate as the NEMS is carried on the same satellite as the DMSP radiometer. The 'H-package' infrared sounder to be flown on future DMSP satellites may satisfy the requirement of acquiring reasonably accurate estimates of M concurrently with 'window' radiances. Shen and Smith (1972) indicate that the SIRS-B sounder provided estimates of M to within ± 20 percent or about ± 0.6 g cm^{-2} where M ~ 3 g cm^{-3}. Referring to Figure 5.2 it is seen that an error in D_w of about ±1°K atm^{-1} could airse from such an uncertainty in M. The results of Shen and Smith suggest that for an accuracy in D_w of about ± 0.5°K atm^{-1} estimates of M from the H-package should have an accuracy of about 10 percent.

5.5 Approximate Estimates

The deficit (D) may be estimated in the absence of soundings of atmospheric parameters. The first method calculates D in terms of observed radiance temperature (T_B), and the second gives mean values of D in terms of mean values of M and U for climatological regions which are roughly homogenous in these parameters. It will be seen that these methods produce relatively crude estimates of D which, nevertheless, are of use in certain types of investigation involving relatively large changes in sea surface temperatures.

5.5.1 The Deficit as a Function of Measured Radiance Temperature

In the absence of all atmospheric data except those indicating the presence of cloud, D may be roughly estimated by the use of an expression in terms of T_B. D may be estimated in this way because radiance temperature is roughly correlated with atmospheric moisture since T_B and M generally decrease as latitude increases and as the height of the viewed surface (i.e., a cloud top) increases. Furthermore, for a given area and season U, and therefore D_o, may be represented by a constant to a

TABLE 5-4

Date and Station	M (Sounding) ($g\ cm^{-2}$)	D_w (Sounding) ($°K\ atm^{-1}$)	M (NEMS) ($g\ cm^{-2}$)	D_w (NEMS) ($°K\ atm^{-1}$)	ΔM ($g\ cm^{-2}$)	ΔD_w ($°K\ atm^{-1}$)	Approximate Distance (km ± 5 km)
4 Jan 1973 Ship 'E'	1.48	1.58	1.00	1.02	0.48	0.56	35 (10)
5 Jan 1973 Bermuda	3.40	4.31	3.29	4.13	0.11	0.18	160 (175)
7 Jan 1973 Bermuda	1.70	1.85	2.02	2.27	-0.32	-0.42	215 (185)
26 Jan 1973 Bermuda	1.46	1.55	1.54	1.65	-0.08	-0.10	100 (75)
31 Jan 1973 Bermuda	0.87	0.87	1.01	1.03	-0.14	-0.16	185 (195)

Comparison of values of integrated water vapor (M) and computed values of the corresponding deficit (D_w) between those calculated from NEMS and radiosonde data. The approximate distance is that between the station and the subsatellite track plus the estimated distance the balloon traveled based upon the mean wind for the lower troposphere (to about 500 mb). The value in parenthesis is the distance from station to track. D_w is computed from the parametric formula ($D \simeq 0.91\ M + 0.105\ M^2$).

sufficient accuracy. The following formula is suggested based partly on work by Smith, et al (1970), but for the 8 to 13 μm window.

$$D_T \simeq (a \ln \frac{100}{310-T_B})^b + C \qquad \text{for } 210 \leq T_B \leq 300$$

where D_T is the value of $D \propto T_B$, a = 1.2, b = 1.8, and C = 6.05° $Katm^{-1}$ for the MODE area. T_B is in degrees K. The above formula gives an estimate of D which is approximately representative of the mean conditions prevailing over an oceanic region where M and U vary relatively little in time and space. Even in the limited area of the MODE region for 13-15 June M varies considerably as may be seen in Table 5.3 causing a consequent variation in D_p of about 2° K atm^{-1} even though T_B changed only about 1°K over the three day period and D_T only a few tenths of a degree.

Figure 5.4 shows D_T as a function of T_B for $250 \leq T_B \leq 300$°K. Parametric values of D are plotted, the thirteen values of D_p of Table 5.3 and one estimate of D for Ship 'E' from Table 5.4.

It can be seen from Figure 5.2 that D_T approximates D_p to about ± 2°K atm^{-1} in the MODE region. A likely accuracy in T_s, excluding the probable systematic bias, would be about 4 to 4.5°K, since D_p may be incorrect by ± 1°K, the uncertainity in T_B arising from the use of a "lookup" table is about ± 1°K, and noise may account for several tenths of a degree even when averaged values of T_B are used.

5.5.2 Statistical Estimate

A statistical estimate of D based on climatological values of M, as well as of U, can be used in the absence of daily soundings of atmospheric parameters. In this method mean values of M ($\overline{M}$) would be found for cliamtologically similar regions over the oceans. It would then be assumed that D equalled its mean value ($\overline{D}$) within each region. $\overline{D}$ would be computed by either the parametric equation or by integration of the equation of radiative transfer.

To assess the validity of the method, $\overline{M}$ and the standard deviation of M (σ_M) were found for the MODE region using thirteen soundings from Ship 'H' (see Table 5.3). It was found that $\overline{M}$ = 3.02 g cm^{-2} and σ_M = 0.64 g cm^{-2}; the corresponding values of D_p for M at $-\sigma_M$, $\overline{M}$, and

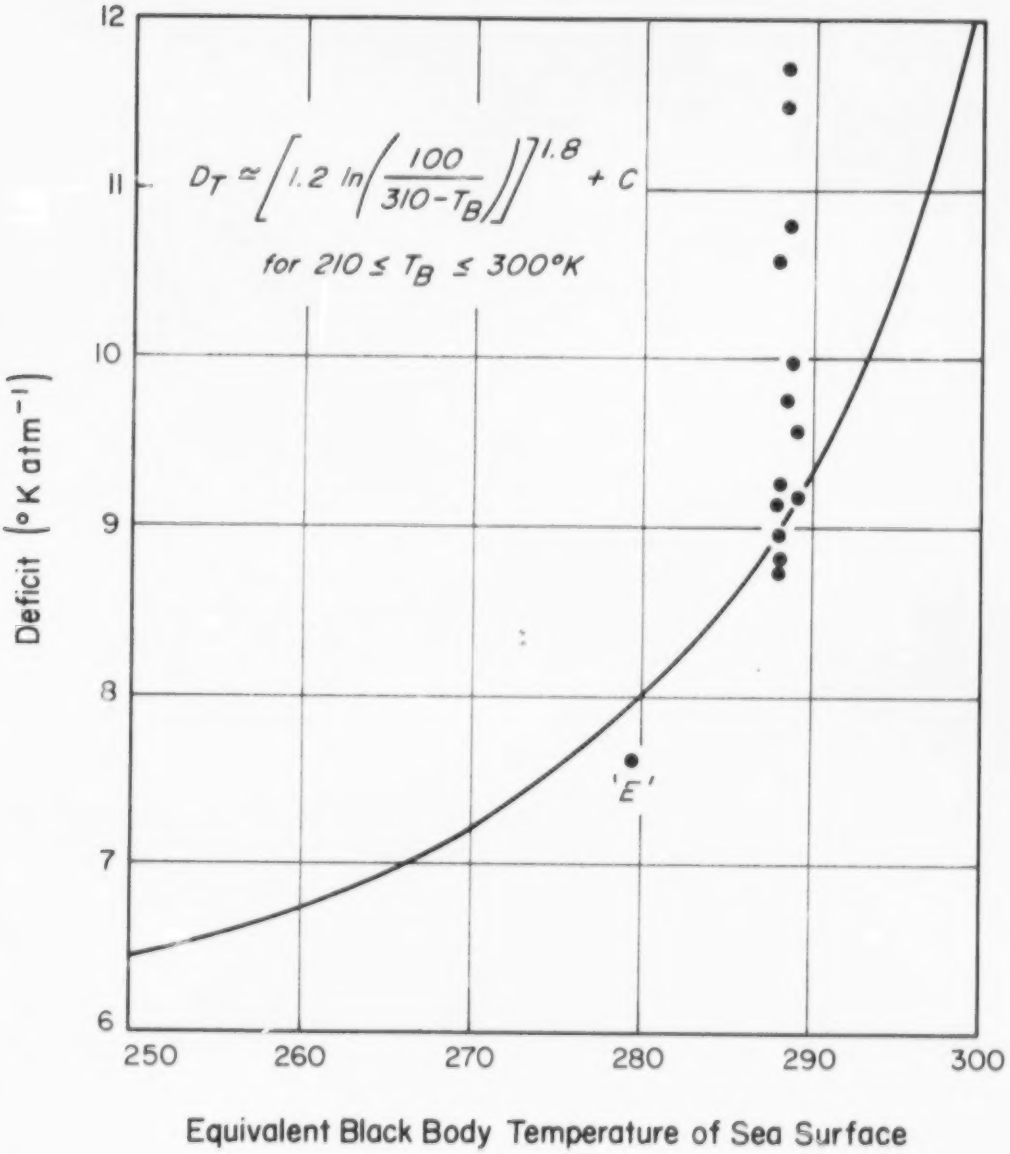

Figure 5.4 The deficit (D_T) as a function of radiance temperature (T_B), and comparison with thirteen values for the MODE region and one value for ship 'E' computed from the parametric formula. $C = 6.05°K\ atm^{-1}$, the value for a Mid-Latitude summer atmosphere (Table 5.1).

$+\sigma_M$ were 8.81, 9.76 and 10.79°K atm^{-1} respectively. Extreme values of M were 2.33 and 4.19 gcm^{-2} with corresponding values of D_p of 8.74 and 11.71°K atm^{-1}. Therefore, a D with an accuracy of about $\pm$ 1.0°K atm^{-1} relative to "daily" values of D_p can be expected for most cases and $\pm$ 2.0 °K atm^{-1} for all but the most extreme examples. The general accuracy of about $\pm$ 1.5°K atm^{-1} is somewhat better than that obtained using the formula for D_T (D as a function of T_B, see above). The likely accuracy in T_s, excluding the probable systematic bias, is about 3.5 to 4°K for reasons given in Section 5.5.1 above.

5.6 Comparison of Computed with Observed Deficits

Values of D derived from the comparison of mean values of equivalent black body temperature ($\overline{T}_B$) of the sea surface with ship measurements of T_s were compared with values computed from the integration of the equation of radiative transfer and the parametric formula. For the initial comparison of satellite and ship measurements digital strip charts of the type described in Section 2 were constructed for an area which included the geographical locations of the ships. By a comparison of cloud patterns the position of each ship was accurately (to within a few tenths of a degree of latitude) transferred from the infrared imagery to the mapped area. The areas containing the ships were then expanded into maps of T_B on a larger scale (100 x 100 scan spots). Corresponding maps of visible brightness values (b) were constructed for the same regions. Three sets of maps were produced for those days (13, 14, 15 June) which had at least two ship reports of sea surface temperature (near 1530Z), a sounding from one of the ships (near 1200Z), and a cloud-free atmosphere over at least some of the area containing the ships. Ship measurements of sea surface temperature were compared with values of $\overline{T}_B$ for each of the three days.

Initially a 10 x 10 scan spot square (enlarged when insufficient data were available) was centered approximately at the geographical location of each ship for each day. Within each such area values of T_B

for scan spots which were roughly determined to be free of clouds with the aid of a manual comparison with the visible data (see Section 4) were tested to see if they were within the likely 'climatological' limits (i.e., $T_{min} < T_B < T_{max}$) based on data from the Marine Climatic Atlas of the World (1969). Also T_B was unlikely to exceed T_s (maximum value measured = 299.0°K) unless a very large (> 10°K too warm) systematic bias had been present in the satellite data or the skin temperature of the ocean exceeded the bulk temperature by more than about 10°K. Therefore, T_{max} was set equal to 299 K° and T_{min} to 285°K. The remaining 'good' values of T_B were averaged to obtain $\overline{T}_B$ for each 'square'.

$\overline{T}_B$ was compared with the corresponding ship measurement of T_s to obtain the temperature difference (ΔT). From ΔT the temperature deficit (D_s) was calculated from $D_s = \Delta T \cos z$, where z = zenith angle. Note that this relationship holds for z < about 66° and fairly well to z < about 75°. D_s from all ships for each day were averaged and the result compared with the value (D_p) computed from the parametric formula to get ΔD_p. $\Delta D_c (= D_c - D_s)$ was computed using the above technique where D_c = D calculated by the numerical integration of the equation of radiative transfer.

Further comparisons were made with three measurements of T_s from ships of opportunity which were taken on 13 June (06Z) and 14 June 1973 (12 and 18Z). Two additional ship measurements which exceeded 300°K (300.8 and 301.0°K) were eliminated. The values of D derived using these ship data were 1.73°K atm^{-1} for 13 June and 5.13°K atm^{-1} for 14 June, the latter value showed reasonable agreement with corresponding D_s values of Table 5-5. The value for 13 June should not be compared with other values of D_s because of the large z (about 80°).

The results from the above comparisons showed significant differences between computed and observed values of D except for the 15 June case (see Table 5-5). However, as noted in Section 4.2 and 4.5 large errors in the satellite data are likely. Furthermore, any agreement between computed and observed values of D closer than about $\pm$ 0.8 or 0.9°K atm^{-1} should be considered as good because of the uncertainty in the categories of T_B. Also the emissivity of the sea surface for the high zenith angles of the 13 and 14 June data (>56°) may cause an underestimate in T_s of > about 1°K. Perhaps of greater importance is that a

TABLE 5-5

Date (June, 1973)	M	D_c	D_p	D_s (Average Value)	ΔD_c (D_c-D_s)	ΔD_p (D_p-D_s)	Sec z (Average)
13	2.91	9.80	9.59	5.95	3.85	3.65	1.8
14	4.19	11.44	11.71	6.80	4.60	4.90	1.5
15	3.54	10.20	10.59	9.90	0.30	0.70	1.2

Comparison of computed with observed values of D. $\Delta D_c = D_c - D_s$ and $\Delta D_p = D_s$. All values of D and ΔD are in °K atm^{-1}. Sounding of 14 June may have passed through a cloud near 750 mb. Values of D_s ΔD_c, and ΔD_p are to the nearest 0.05°K.

"systematic" bias of up to 5°K may exist in the data for any given T_B; this error may vary somewhat with temperature (private communication with Westinghouse personnel, 1975). If we assume a systematic bias of +5°K, for all of the data examined then better agreement is reached for 13 and 14 June and poorer agreement for 15 June as shown in Table 5-6. These results represent an overall improvement over those of Table 5-5.

Finally in an attempt to determine what relationship, if any, existed between ΔT (= $T_s - T_B$) and the secant of the zenith angle Figure 5-5 was constructed in which values of D_s for each ship for all days, including the three ships of opportunity, were plotted as a function of sec z. From this figure it is evident that there is no clear relationship in these data, contrary to what would be expected from past work and theory (see also Cogan and Willand, 1974 and Cogan, 1972). Unfortunately, no explanation for this discrepancy could be found; no effort was made to correct for z at EPRF and, according to documentation available to EPRF, no such correction was made onboard the satellite (private communication, 1975). Table 5-7 shows the results of comparisons between computed and observed values of D when it is assumed that ΔT is independent of z (i.e., $\Delta T = D_s$). In this case, better agreement is reached than in either Table 5-5 or 5-6.

It must be remembered that unknown atmospheric variations may account for a part of the aforementioned discrepancies. For example, ozone amount and distribution were assumed constant at their climatological averages. However, total ozone content may vary by 15 or 20 percent over several days causing a difference in D of perhaps 1/2°K atm^{-1}, and changes in the vertical distribution over the same period may produce a further change in D of, say, 1/2°K atm^{-1} (see also Sections 5.1 - 5.3). Atmospheric aerosols can vary in amount and distribution causing a further uncertainty in D of perhaps 0.3°K atm^{-1} (see Table 5-2). Also a discrepancy in M for 14 June may have occurred as a consequence of the likely passage of the radiosonde through cloud near 750 mb.

The comparisons presented in Tables 5-5 through 5-7 suggest that the DMSP data cannot be used for obtaining values of T_s if an absolute accuracy of < about 5°K is required. However, information on gradients

TABLE 5-6

Date (June, 1973)	M	D_c	D_p	D_s (Average Value)	ΔD_c (D_c-D_s)	ΔD_p (D_p-D_s)	Sec z (Average)
13	2.91	9.80	9.59	8.65	1.15	0.90	1.8
14	4.19	11.44	11.71	10.15	1.30	1.55	1.5
15	3.54	10.20	10.59	13.90	-3.70	-3.35	1.2

Comparison of computed with observed values of D assuming a systematic bias of 5°K (too warm) $\Delta D_c = D_c - D_s$ and $\Delta D_p = D_p - D_s$. All values of D and ΔD are in °K atm^{-1}. Sounding of 14 June may have passed through a cloud near 750 mb. Values of D_s, ΔD_c, and ΔD_p are to the nearest 0.05°K.

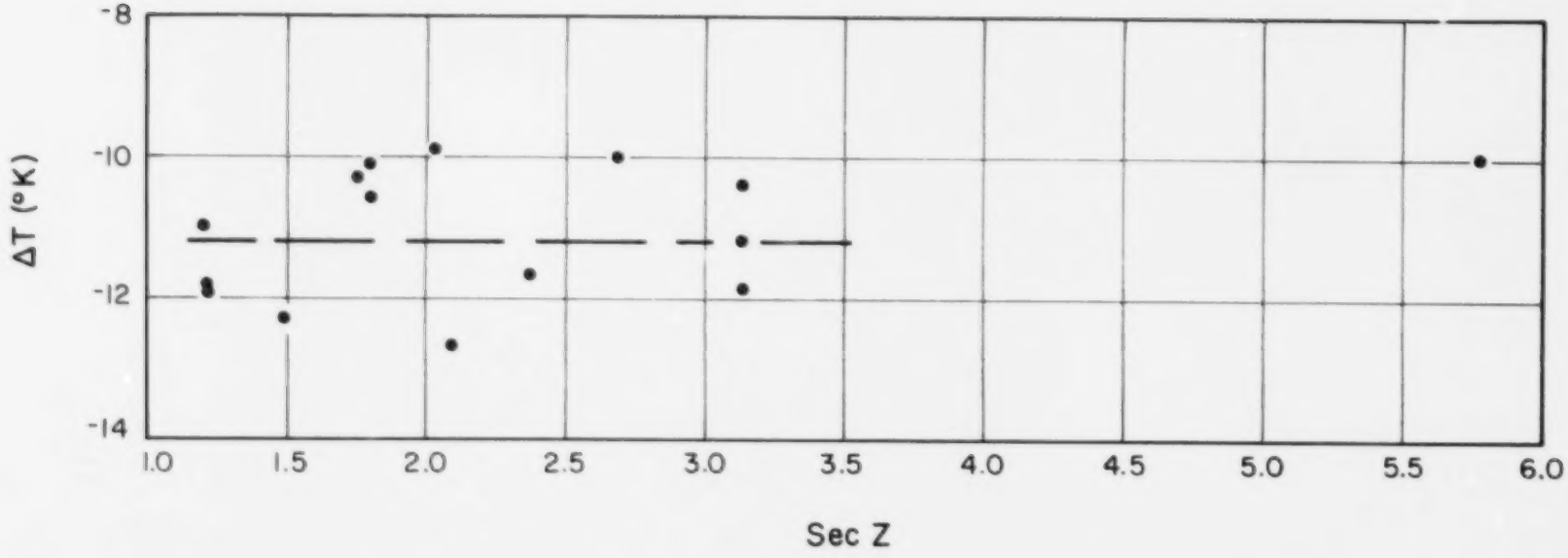

Figure 5.5 ΔT $(=T_s - \overline{T}_B)$ as a function of sec Z. Note the apparent lack of any relationship between ΔT and sec Z (see text).

TABLE 5-7

Date (June, 1973)	M	D_c	D_p	D_s (Average Value)	ΔD_c (D_c-D_s)	ΔD_p (D_p-D_s)	S c z (Average)
13	2.91	9.80	9.59	10.85	-0.95	1.30	1.8
14	4.91	11.44	11.71	10.90	0.55	0.85	1.5
15	3.54	10.20	10.59	10.20	0.00	0.35	1.2

Comparison of computed with observed values of D assuming that $\Delta T = D_s$. $\Delta D_c = D_c - D_s$ and $\Delta D_p = D_p - D_s$. All values of D and ΔD are in °K atm^{-1}. Sounding of 14 June may have passed through a cloud near 750 mb. Values of D_s, ΔD_c, and ΔD_p are to the nearest 0.05°K.

may be extracted from the data limited only by random error and uncertainty in the T_B categories. Referring to Section 3.5 it seems likely that gradients in T_s of > 2°K should be detectable provided that they do not reverse themselves over distances less than 20 km, since a sufficient number of scan spots must be averaged to minimize noise (see also Section 6.4). The constraint of a "one-way" gradient for 20 km may be reduced to about 10 to 15 km for entirely cloud-free areas because few, if any, scan spots would be assumed to be cloud contaminated. Noise, for example, may cause low values of T_B to occur in a cloud-free region.

6. MAPPING RESULTS

The work of this section does not indicate how accurately T_s may be inferred using current DMSP data, but serves to illustrate the mapping technique under the assumption that ΔT, the difference between satellite values of T_B and ship measurements, is independent of the zenith angle (z) for reasons given in Section 5.6. Maps of T_s for 13-15 June 1973 were produced using the observed value of ΔT for each day, thereby eliminating the effect of systematic bias. A map of T_s for 13 June was prepared where $\Delta T = D_s \sec z$ and D_s is the observed deficit which may be compared with the map for that date with ΔT = constant. For the 13 June case two other maps at higher effective resolutions were prepared; for these maps ΔT = constant. These maps may be compared with the full size map for 13 June that has a constant correction for attenuation. A composite mapping technique is suggested, based on that proposed by Fogan and Willand (1974), and limitations are discussed on the quality of information that can be obtained.

6.1 Comparison of Daily Maps

Maps of T_s (Figures 6.1a, 6.2a, and 6.3a) were produced for 13-15 June 1973 where ΔT was assumed constant for each day and therefore independent of z. Accompanying maps of N (Figures 6.1b, 6.2b, and 6.3b) were prepared that give the population of 'good' values of T_B (see Section 5.6) used to compute each mapped T_s. Values of N give an idea of the cloudiness within each "box" of scan spots and the reliability to be placed on each mapped T_s (e.g., a mapped T_s with N = 1 or 2 is more likely to deviate significantly from the actual value than one with N = 90).

Differences between adjacent values of T_s can provide a measure of the effect of noise if the sea surface is nearly uniform in T_s and no significant horizontal variation exists in the atmosphere (i.e. resultant attenuation is constant to 0.1 or 0.2°K atm^{-1}). These criteria are likely to occur in the MODE region in cloud-free areas. The size of the fluctuations in T_s may be compared with values of N in order to roughly estimate the effect of noise on T_s for different N. Noise may be better estimated when the initial sample size is decreased from 100

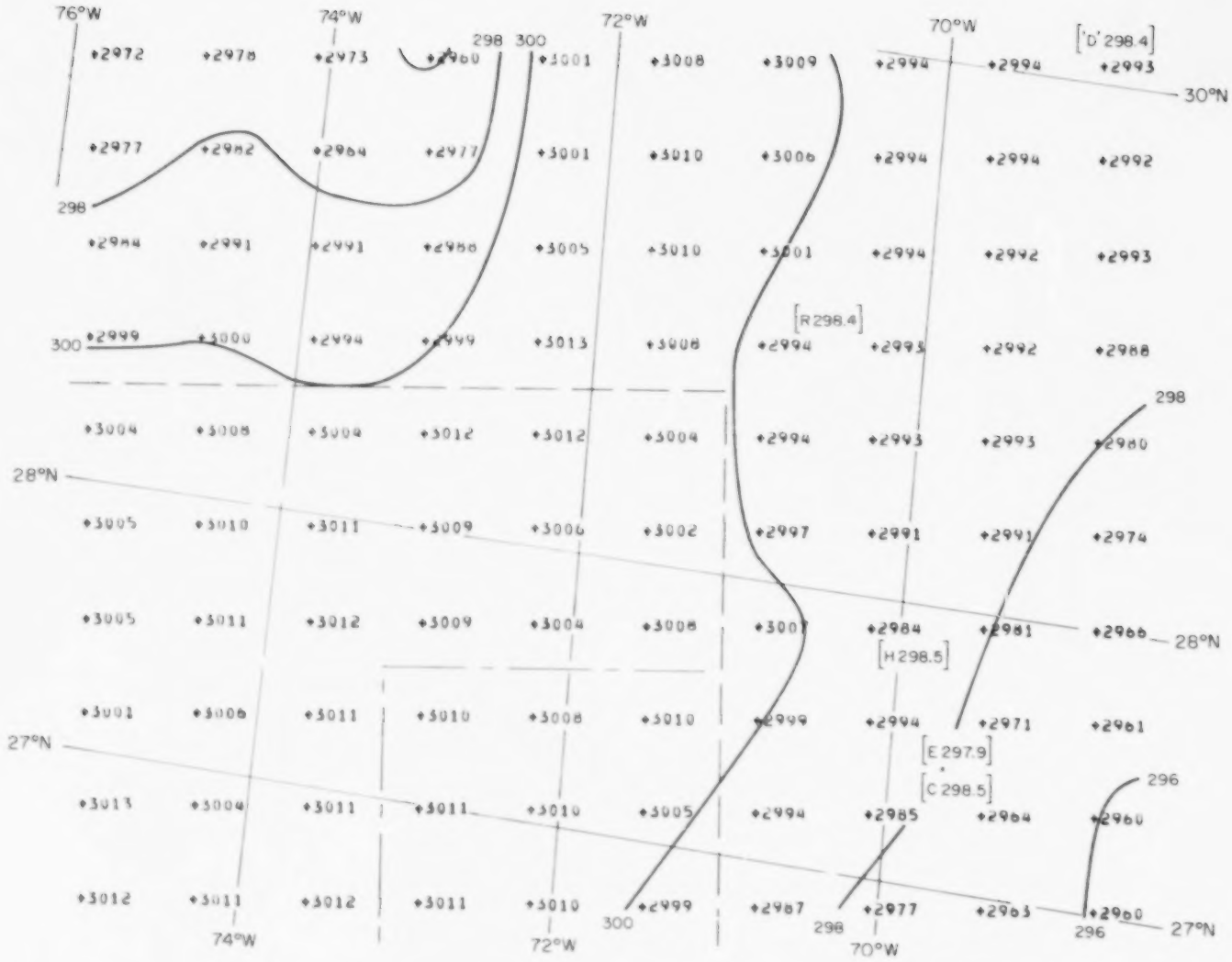

Figure 6.1a Map of T_s for 13 June 1973. Mapped values are degrees K x 10, and ship measurements are enclosed in brackets and placed at the appropriate locations. Approximate geographical coordinates are drawn as are isotherms for every even whole degree. Areas of higher resolution maps, Figures 6.5a and 6.6a, are outlined to the lower left. Observed value of ΔT (= 10.8°K) is used to correct for atmospheric attenuation.

+ 7	+ 16	+ 11	+ 1	+ 62	+ 97	+ 100	+ 59	+ 97	+ 100
+ 18	+ 19	+ 12	+ 26	+ 78	+ 96	+ 100	+ 81	+ 100	+ 99
+ 65	+ 87	+ 50	+ 54	+ 94	+ 100	+ 77	+ 92	+ 87	+ 100
+ 95	+ 86	+ 82	+ 86	+ 100	+ 99	+ 77	+ 80	+ 83	+ 90
+ 96	+ 96	+ 93	+ 100	+ 100	+ 83	+ 81	+ 76	+ 100	+ 100
+ 81	+ 98	+ 100	+ 99	+ 90	+ 85	+ 98	+ 94	+ 100	+ 92
+ 97	+ 99	+ 99	+ 94	+ 73	+ 99	+ 94	+ 60	+ 90	+ 33
+ 87	+ 78	+ 99	+ 95	+ 97	+ 100	+ 91	+ 96	+ 52	+ 11
+ 100	+ 60	+ 92	+ 100	+ 100	+ 89	+ 89	+ 87	+ 83	+ 20
+ 80	+ 71	+ 68	+ 89	+ 85	+ 73	+ 82	+ 85	+ 49	+ 16

Figure 6.1b Population map for 13 June where each plotted value is the number, N, of "good" values used to compute each mapped T_s. This map corresponds to Figure 6.1a.

Figure 6.2a Map of T_s for 14 June constructed in the same manner as Figure 6.1a. T_s is set to 0 when the corresponding N = 0. ΔT = 10.9°K.

Figure 6.2b Population map for 14 June. This map corresponds to Figure 6.2a.

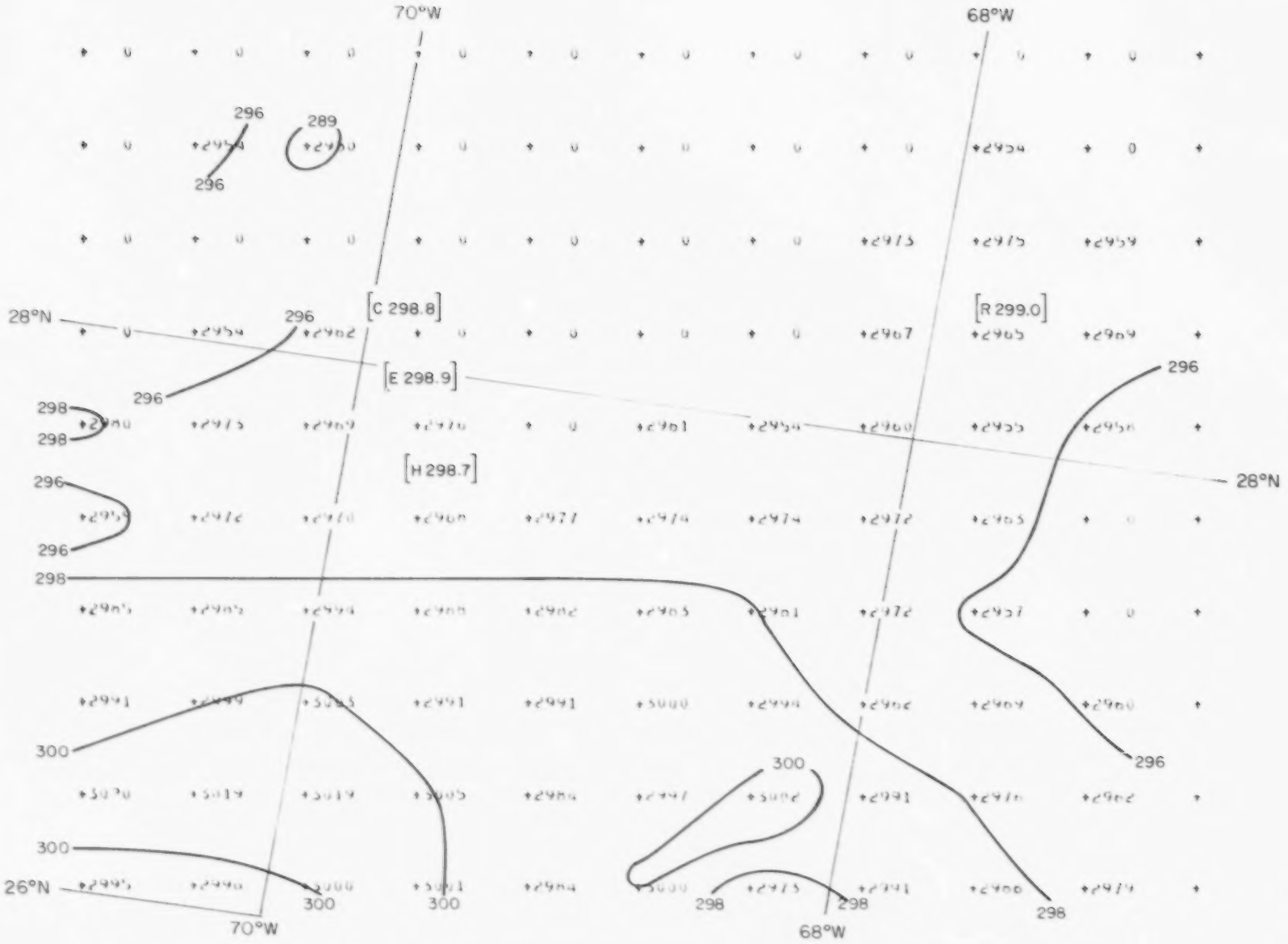

Figure 6.3a Map of T_S for 15 June constructed in the same manner as Figure 6.1a and 6.2a. $\Delta T = 10.2°K$.

0	0	0	0	0	0	0	0	0	0
0	1	7	0	0	0	0	0	1	0
0	0	0	0	0	0	0	44	62	5
0	1	2	0	0	0	0	60	84	45
51	41	54	15	0	7	3	27	21	49
23	80	74	32	10	22	73	93	57	0
95	95	100	98	84	76	93	82	54	0
75	97	98	94	78	99	96	27	52	5
87	95	100	96	37	87	90	48	47	16
43	71	100	97	73	93	29	64	85	52

Figure 6.3b Population map for 15 June. This map corresponds to Figure 6.3a.

to 25 or 9 scan spots and a smaller (and therefore more likely to be uniform) area of the sea surface is examined (see Section 6.3).

On these maps, values of T_s with accompanying values of $N < 5$ appear unreliable, possibly as a consequence of noise or of the failure of the computer algorithm to eliminate cloud contaminated data within climatological limits. All three maps of T_s indicate a slight decrease in T_s from south to north, and from west (left) to east (right) along the bottom half (generally south of 28°N). A comparison of ship measurements with nearby satellite derived values shows that T_s was estimated to a mean accuracy of about 1.2°K, with "daily" mean accuracies of about 0.9, 0.8, and 1.8°K for 13, 14, and 15 June respectively. The values for 15 June may be too high because ship CHAIN with an "accuracy" of 2.6°K was located under an extensive cloud cover and N was < 5 for the closest mapped satellite value. As noted in Section 4.5, an accuracy of better than about 0.9°K may not be realistic with DMSP 8-13 μm data, and furthermore, the use of a constant value of ΔT enables T_s to be mapped at almost the best realistic accuracy. Note that the values of ΔT used here are the "observed" values, and, therefore, any systematic bias would not affect the computation of T_s. To estimate the accuracy of T_s inferred using computed values of ΔT, where $\Delta T = D_c$ or D_p, refer to Table 5.7 and add the appropriate ΔD to the satellite T_s. Note that in Table 5.7 the observed value of $\Delta T = D_s$.

6.2 Effect of a Variable Zenith Angle

The comparison between the two full sized maps for 13 June demonstrate the consequence of the apparent lack of any relationship between ΔT and z. Figure 6.4 was constructed similarly to Figure 6.1a but with ΔT as a function of z where $D_s = 5.25°K\ atm^{-1}$ (see Table 5.6) and a systematic bias of 5°K (too warm) was assumed. This map covers the same area as Figure 6.1a, but the resultant pattern of T_s is quite different in that there is an increasing gradient of T_s from left to right (roughly west to east). A small gradient of T_s from north to south shows up on both maps, and unrealistically high values occur on the right side and unlikely low values on the left side of Figure 6.4. Note that the right side of the map is only a few scan spots from the edge of the earth

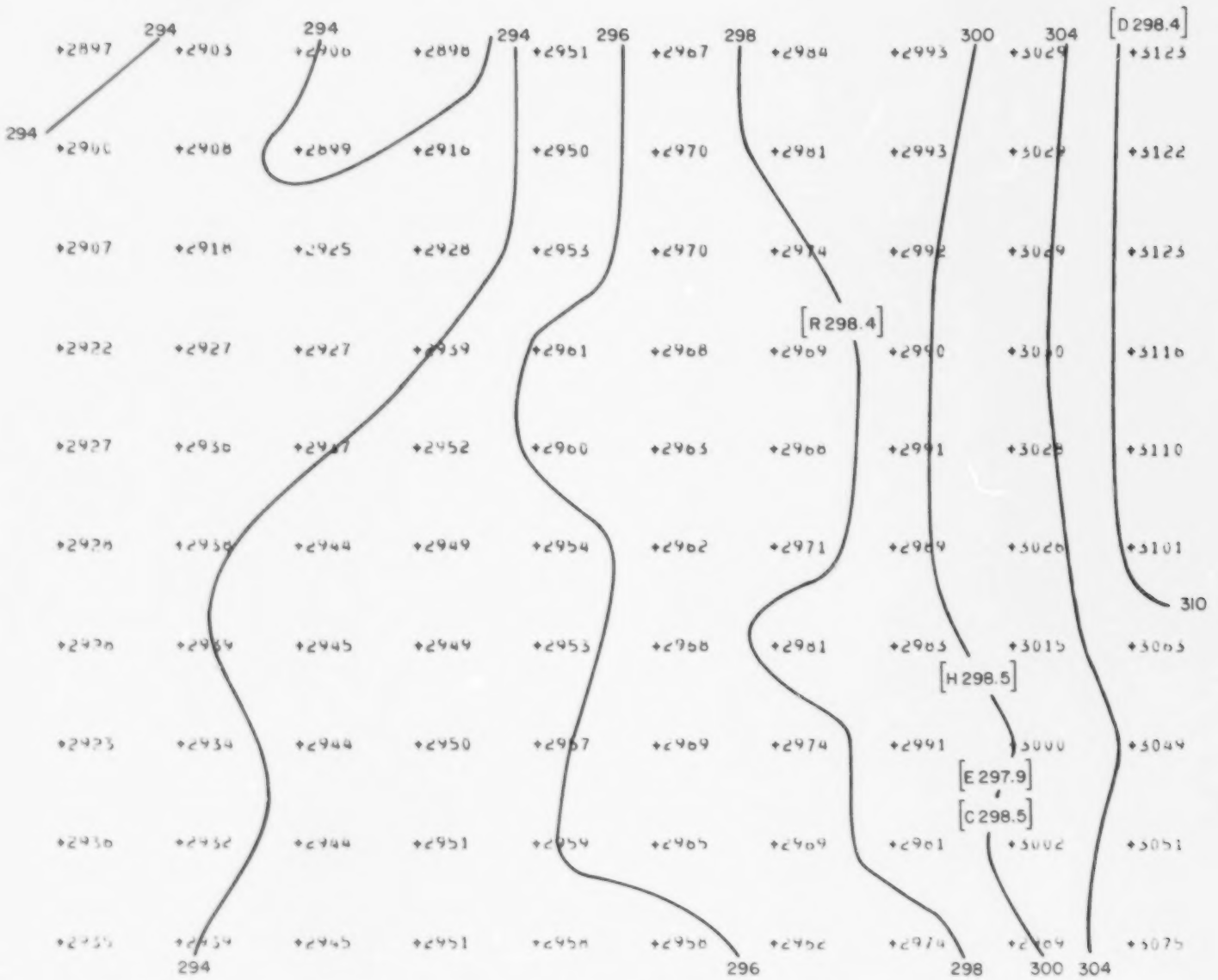

Figure 6.4 Map of T_s for 13 June constructed in a similar manner as Figure 6.1a, but with a different correction technique for atmospheric attenuation. Here $\Delta T = D_s \sec z$ where $D_s = 5.25°K\ atm^{-1}$, and a systematic bias of 5°K (too warm) was assumed. Compare with Figure 6.1a where ΔT = constant and no bias was assumed.

scan. If we assumed that no systematic bias was present in the data then the values to the left would be more reasonable, but those on the entire right half would be much too high, especially along the right edge.

6.3 Variation of Effective Resolution

Maps of T_s and N at several effective resolutions were prepared to illustrate the increase in detail of the T_s field with higher resolution. Figures 6.5a and 6.6a are maps for 13 June having sizes of 60 x 60 and 30 x 30 scan spots respectively; 6.5b and 6.6b are the corresponding maps of N. The effective resolutions of these maps are 5 x 5 and 3 x 3 scan spots that represent areas of about 22 x 22 and 13 x 13 km near the sub-satellite track, but considerably larger areas at the scan angles of these data (nadir angles ≈ 52°).

As expected, a major difference between these maps is the apparent greater detail in the field of T_s as the effective resolution increases, probably arising as a consequence of less smoothing of the data used to compute each mapped T_s. Compare, for example, Figure 6.1a and 6.6a. Another noticeable result is the apparent lack of significant noise in T_s for small N ($4 \leq N \leq 9$). This effect may occur because of either or both of the following:

a. Only data for an extensive cloud-free region (i.e., little T_s gradient) were selected for the work of this section, or

b. Each T_B represents a range of temperature of about 1.7°K, thereby tending to mask noise.

The results of this section suggest the use of a composite mapping technique similar to that suggested by Cogan and Willand (1974) for NOAA-2 data. In their method, a map at a lower effective resolution is overlaid by a map at a higher one so that the maximum areal coverage is maintained while allowing more detail of the field of T_s for almost entirely cloud-free regions. Because of the apparent lack of significant (> 0.5°K) noise when N is small, the higher effective resolution for DMSP data can be 3 x 3 scan spots, representing an area of about 13 x 13 km near the sub-satellite track. The work of this section also

Figure 6.5a Map of T_s for 13 June constructed in a similar manner as Figure 6.1a, but for an effective resolution of 5 x 5 scan spots. Note location of this map on Figure 6.1a. Area of Figure 6.6a is outlined to the lower right, and $\Delta T = 10.8°K$.

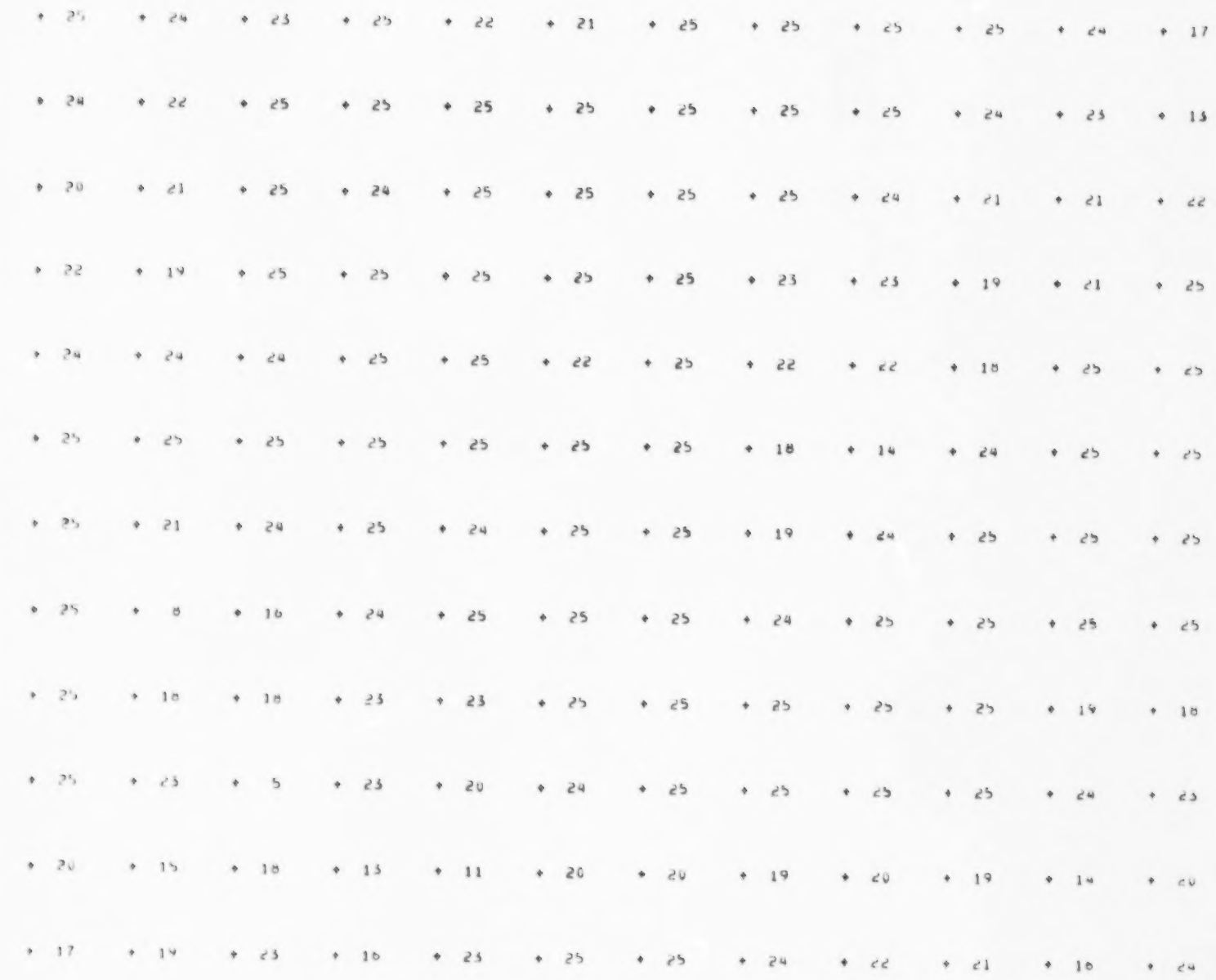

Figure 6.5b Population map for 13 June. This map corresponds to Figure 6.5a.

Figure 6.6a Map of T_s for 13 June constructed in a similar manner as Figures 6.1a and 6.5a, but for an effective resolution of 3 x 3 scan spots. Note location of this map on Figures 6.1a and 6.5a. $\Delta T = 10.8°K$.

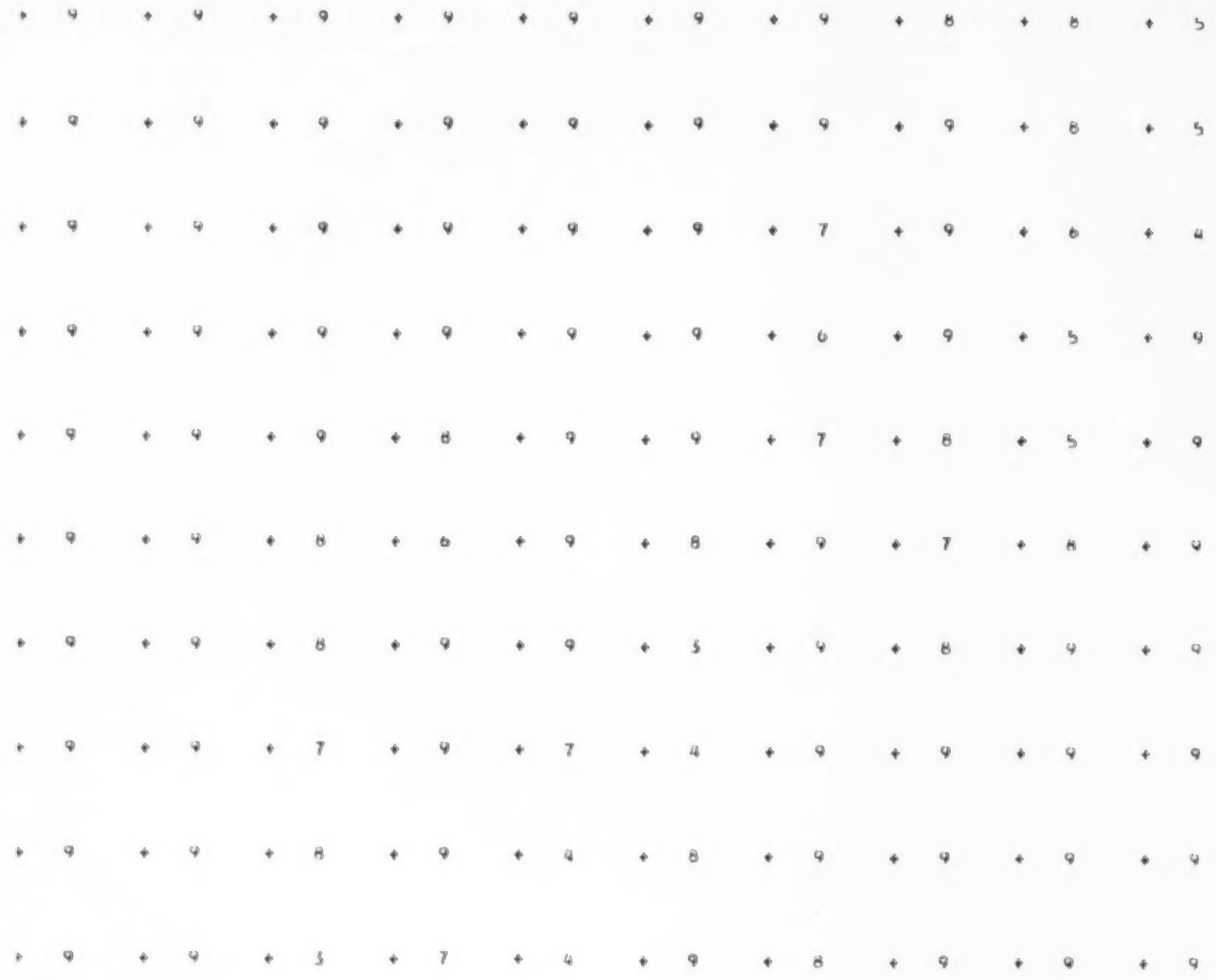

Figure 6.6b Population map for 13 June. This map corresponds to Figure 6.6a.

indicates that for entirely cloud-free regions, noise is reduced considerably when N = 4, thereby permitting the use of an effective resolution of 2 x 2 scan spots, about 9 x 9 km, under ideal conditions. Unfortunately, as will be discussed in Section 6.4, the improvement in effective resolution of DMSP relative to NOAA-2 data does not necessarily imply an improvement in accuracy.

6.4 Quality and Limitations

The use of DMSP data for detailed mapping to T_s is severely curtailed by several factors. One of these is the lack of any clear relationship between ΔT and z. This liability may be overcome at least partially by considering only data near the sub-satellite track. The above discrepancy is discussed more fully in Sections 5.6 and 6.2.

Another potentially serious problem is the possible "systematic" bias of up to 5°K, which may vary somewhat with temperature, that is presently unknown and not documented to the best knowledge of the authors (private communications with personnel at EFRF, Westinghouse Electric Corporation, AFCRL and Keesler AFB, 1974 and 1975). This error may be roughly estimated, but its actual magnitude may be obscured by the aforementioned apparent lack of any definite relationship between z and ΔT.

Even if all errors in the data were completely accounted for, there would be an additional limitation arising from the large size (1.7 to 1.8°K) of the T_B categories (see Sections 3.2 and 3.5). The effect of this large magnitude is to permit a range of T_B, and therefore of T_s, of about 1.7°K to occur for a region ostensibly uniform to T_s. Spatial temperature changes of < 1.7°K could be obscured and an indicated change of, say, one such temperature category may indicate an actual change of from 0.1 to 3.4°K. Where T_s is not uniform, but two or three different values within climatological limits describe the field of T_s, then an averaging technique such as the one discussed in Section 5.6 may reduce somewhat the uncertainty in T_s and its gradient (see also Section 3.5).

In summary, we may note the following:

a. DMSP data can provide estimates of T_s at a relatively high effective resolution, but

b. a large uncertainty exists for any mapped T_s or its gradient as a result of the large size of the T_B categories, the possible "systematic" bias, and the apparent independence of ΔT and z.

If processing of the data is fully understood and all "systematic" bias is accounted for, then T_s may be mapped to an accuracy of perhaps $\pm$ 2°K (uncertainty of T_B category plus ΔD from Table 5.7), possibly better under certain ideal condidtions. Furthermore, if the "systematic" bias is unknown but truly constant in space and time, then the gradient of T_s may be estimated to $< \pm$ 3.5°K per effective resolution distance (= length of one "side" of a "box" of scan spots) with a mean accuracy of about half that size.

7. CONCLUSION

An accuracy of about ± 2°K in T_s is possible using data from the 8-13 μm radiometer carried on DMSP satellites provided that processing of the data is fully understood and all systematic bias have been accounted for. Gradient information may be extracted from the data even when systematic bias is unknown. However, the best assured accuracy is only about ± 3.5°K per unit distance; a likely accuracy is about ± 2°K per unit distance. Under certain conditions (Sections 4.5 and 6.4), the above accuracies may be improved through the use of the averaging techniques discussed in this report.

Sources of the relatively poor accuracy compared with that found for NOAA-2 data may include the following:

a. the large size of the categories of T_B,

b. a systematic bias of up to 5°K,

c. a lack of any clear relationship between z and ΔT,

d. and the choice of a spectral interval that includes the strong ozone band centered near 9.6 μm and extends into wings of the water vapor and carbon dioxide bands centered near 6.7 and 15 μm.

Uncertainties in the data prevented a conclusive comparison between observed and computed values of the deficit, but some of the results of Section 5.6 (see Table 5.7) suggested that D may be computed to about ± 1°K atm^{-1} for the so-called 8-13 μm window. Additionally, a parametric formula gave values of D to < ± 0.6°K atm^{-1} of the values computed by numerical integration of the equation of radiative transfer for 13 of 14 cases.

The effective resolution of each mapped T_s inferred from DMSP data represents a significant improvement over that obtained by Cogan and Willand (1974) using scanning radiometer data from the NOAA-2 satellite. For entirely cloud-free areas the effective resolution is about 13 x 13 km (3 x 3 scan spots) near the sub-satellite track. This relatively high resolution could be important in the monitoring of smaller phenomena, such as local upwelling, especially when the accuracy of the

data from possible future DMSP radiometers equals or surpasses the ±1°K found by Cogan and Willand for NOAA-2 data.

Under the assumption that better data will be forthcoming from a future DMSP radiometer a composite mapping technique was developed that utilizes maps of T_s at two or more effective resolutions. A coarse effective resolution permitted the mapping of most of the sea surface, except areas under extensive cloud cover, and a finer resolution provided greater detail of patterns of T_s for those areas almost entirely cloud-free. This automated mapping algorithm may be used with data from future DMSP satellites since it is fairly general and only minor modifications would be required.

REFERENCES

Bignell, K. J., 1970: Water-Vapor Infrared Continuum, Quart, J. R. Met. Soc. 9(6), 390-403.

Bignell, K., Saiedy, F., and Sheppard, P. A., 1963: On the Atmospheric Infrared Continuum, J. Opt. Soc. Amer., 53, 466-479.

Buettner, K, J. K., and Kern, C. D., 1965: The Determination of Infrared Emissivity of Terrestrial Surfaces, J. Geophys. Res., 70, 1329-1337.

Bruce, J. G., and Firing, E., 1974: Temperature Measurements in the Upper 10 m with Modified Expendable Bathythermograph Probes, J. Geophys. Res., 79(27), 4110-4111.

Cogan, J. L., 1972: Interpretation and Utilization of Satellite Measurements of Sea Surface Temperature, Ph.D. Thesis, Dept. of Meteor., Imperial College of Science and Tech., University of London, England, 103 pp.

Cogan, J. L., and Willand, J. H., 1974: Mapping of Sea Surface Temperature by the NOAA-2 Satellite, Tech. Rpt. (EPRF TR-6-74 (ERT)) Prepared for Environ. Prediction Res. Fac., Naval Post Graduate School Under Contract N66314-73-C1749, Environmental Research & Technology, Inc., Concord, Massachusetts, 72 pp.

Deirmendjain, D., 1964: Scattering and Polarization Properties of Water Clouds and Hazes in the Visible and Infrared, Appl. Opt., 3 (2), 187-196.

Dutsch, H. D., 1974: "The Ozone Distribution in the Atmosphere", Can. J. Chem., Vol. 52, No. 8, 1491-1504.

Ewing, G. C. and McAlister, E. D., 1960: On the Thermal Boundary Layer of the Ocean, Science, 131, 1374-1376.

Hanson, K. J., and Poindexter, M. F., 1972: Attenuance of Broad-Band Solar Irradiance in the Ocean, Conference on Atmospheric Radiation (AMS). Fort Collins, Colorado, 165-168.

Martin, D. W. and Scherer, W. D., 1973: Review of Satellite Rainfall Estimation Methods, Bull. of Amer. Met. Soc. 54(7), 661-674.

Maul, G. A. and Sidran, M., 1973: Atmospheric Effects on Ocean Surface Temperature Sensing from the NOAA Satellite Scanning Radiometer, Geophys. Res. 78, (12), 1909-1916.

McAlister, E. D., and McLeish, W., 1969: Heat Transfer in the Top mm of the Ocean, J. Geophys. Res., 74, 3408-3414.

McClatchey, R. A., Fenn, R. W., Selby, J. E. E., Volz, F. E., Garring J. S., 1972: Optical Properties of the Atmosphere (Third Edition), AFCRL-72-0497, Environmental Research Papers, No. 411, Air Force Cambridge Research Laboratories, L. G. Hanscom Field, Bedford, Mass., 108 pp.

Nimbus 5 User's Guide, 1972: ERTS/Nimbus Project, Goddard Space Flight Center, NASA, Greenbelt, Md., 162 pp.

Platt, C. M. R., 1972: Airborne Infrared Radiance Measurements (10 to 12 Micron Wavelength) off Tropical East Coast Austrailia, J. Geophys. Res., 77, 1597-1609.

Prabhakara, C., Dalu, G., and Hunde, V. G., 1974: Estimation of Sea Surface Temperature from Remote Sensing in the 11 to 13 μm Window Region, J. Geophys. Res., 79(33), 5039-5044.

Rao, P. K., 1975: Picture of the Month - "Invisible" Cirrus Clouds in NOAA-2 Imagery, Mon. Wea. Rev. Vol. 103, 72-77.

Salomonson, V. V., 1974: Advances in Water Resources Monitoring from Space X-913-74-44, Goddard Space Flight Center, Greenbelt, Maryland, 18 pp.

Selby, J. E. A., McClatchey, R. M., 1972: Atmospheric Transmittance from 0.25 to 28.5 μm: Computer Code LOWTRAN 2, AFCRL Environmental Research Paper, No. 427, AFCRL-72-0745, L. G. Hanscom Field, Bedford, Massachusetts, 77 pp.

Shen, W. C., Smith, W. L., 1972: "Statistical Estimation of Precipitable Water with SIRS-B Water Vapor Radiation Measurements: Preprint of Conf. on Atmos. Radiation, Sponsored by American Met. Soc., Fort Collins, Colorado, 145-151.

Smith, S., Rao, P., Koffler, R., and Curtis, W., 1970: The Determination of Sea Surface Temperature from Satellite High Resolution Infrared Window Radiation Measurements, Mon. Wea. Rev., 98(8), 604-611.

Spangler, M. J., 1974: What's the Weather Down There?, Preprint from the October 1974 issue of Westinghouse Engineer, Preprint 186, 10 pp.

Staelin, D. H., Barrett, A. H., Waters, J. W., Barath, F. T., Johnson, E. J., Rosenkranz, P. W., Gaut, N. E., and Lenoir, W. B., 1973: Microwave Spectrometer on the Nimbus 5 Satellite: Meteorological and Geophysical Data, Science, Vol. 182, 1339-1341.

Stevenson, M. R., Miller, R. F., and LaViolette, P. E., 1972: Oceanographic Meteorological, Satellite, and Aircraft Observations for Project Little Window 2: May 1971, Inter-American Tropical Tuna Commission, Data Report No. 5, La Jolla, California, 508 pp.

Williamson, E. J., 1970: The Accuracy of the High Resolution Infrared Radiometer on Nimbus II, NASA Tech. Note: D-5551, Goddard Space Flight Center, Greenbelt, Md., 14 pp.

Wu, M-F, 1973: Observation and Analysis of Trace Constituents in the Stratosphere, Tech. Rpt. Prepared for Dept. of Transportation, CIAP Program, Under Contract DOT-OS-20217, Environmental Research and Technology, Inc., Lexington, Massachusetts, 218 pp.

Wu, M-F, 1974: Trace Constituents in the Stratosphere, Tech. Rpt. Prepared for Dept. of Transportation, CIAP Program, Under Contract DOT-OS-20217, Environmental Research and Technology, Inc., Concord, Massachusetts, 102 pp.